CONTRACT REPORT S-71-10

INVESTIGATION OF AIR INDUCED GROUND SHOCK EFFECT RESULTING FROM VARIOUS EXPLOSIVE SOURCES

Report 2

INFLUENCE OF CONSTITUTIVE MODELS ON GROUND MOTION PREDICTIONS

by

Melvin L. Baron, Ivan Nelson, Ivan Sandler

November 1971

Sponsored by Defense Atomic Support Agency
Nuclear Weapons Effects Subtask SB209

Conducted for U. S. Army Engineer Waterways Experiment Station, Vicksburg, Mississippi

Under Contract No. DACA39-69-C-0022

By Paul Weidlinger, Consulting Engineer, New York, New York

ARMY-MRC VICKSBURG, MISS

UNCLASSIFIED
Security Classification

DOCUMENT CONTROL DATA - R & D

(Security classification of title, body of abstract and indexing annotation must be entered when the overall report is classified)

1 ORIGINATING ACTIVITY (Corporate author)	2a. REPORT SECURITY CLASSIFICATION
Paul Weidlinger, Consulting Engineer New York, New York	Unclassified
	2b. GROUP

3 REPORT TITLE

INVESTIGATION OF AIR INDUCED GROUND SHOCK EFFECT RESULTING FROM VARIOUS EXPLOSIVE SOURCES - REPORT 2 - INFLUENCE OF CONSTITUTIVE MODELS ON GROUND MOTION PREDICTIONS.

4. DESCRIPTIVE NOTES (Type of report and inclusive dates)

Report 2 of a series.

5 AUTHOR(S) (First name, middle initial, last name)

Melvin L. Baron, Ivan Nelson and Ivan Sandler.

6. REPORT DATE	7a. TOTAL NO. OF PAGES	7b. NO. OF REFS
November 1971	63	15

8a. CONTRACT OR GRANT NO.	9a. ORIGINATOR'S REPORT NUMBER(S)
DACA39-69-C-0022 b. PROJECT NO. c. Nuclear Weapons Effects Subtask SB209 d.	9b. OTHER REPORT NO(S) (Any other numbers that may be assigned this report) Waterways Experiment Station Contract Report S-71-10, Report 2

10. DISTRIBUTION STATEMENT

Approved for public release; distribution unlimited.

11. SUPPLEMENTARY NOTES	12. SPONSORING MILITARY ACTIVITY
Prepared under contract for U.S. Army Engineer Waterways Experiment Station, Vicksburg, Mississippi.	Defense Atomic Support Agency Washington, D.C.

13. ABSTRACT

In recents years, the development of mathematical models for the study of ground shock effects in soil and/or rock media has made important progress. Currently, three basic types of advanced models have been studied: (a) elastic-ideally plastic models, (b) variable moduli models, and (c) elastic-nonideally plastic capped models. This paper is the first part of an investigation which is aimed at studying the behavior of the different types of models in ground shock problems.

The ground shock response in the superseismic range of a one megaton air burst on a homogeneous half-space of a soil is considered. Each of the three types of models, was fitted to laboratory test data and calculations were made for each case. Generally, the results from all three models are comparable only when the stress paths in uniaxial strain are comparable for complete load-unload cycles. When this is not so, major differences occur in the lateral motions and stresses.

DD FORM 1 NOV 68 1473 REPLACES DD FORM 1473, 1 JAN 64, WHICH IS OBSOLETE FOR ARMY USE.

UNCLASSIFIED
Security Classification

14. KEY WORDS	LINK A		LINK B		LINK C	
	ROLE	WT	ROLE	WT	ROLE	WT
Ground Shock						
Mathematical Models						
Elastic-Ideally Plastic						
Variable Moduli						
Elastic-Nonideally Plastic						
Stress Path						

CONTRACT REPORT S-71-10

INVESTIGATION OF AIR INDUCED GROUND SHOCK EFFECT RESULTING FROM VARIOUS EXPLOSIVE SOURCES

Report 2

INFLUENCE OF CONSTITUTIVE MODELS ON GROUND MOTION PREDICTIONS

by

Melvin L. Baron, Ivan Nelson, Ivan Sandler

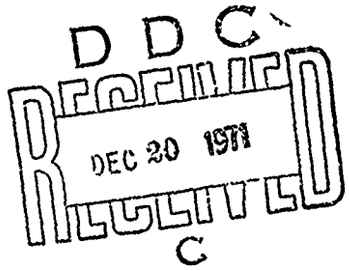

November 1971

Sponsored by Defense Atomic Support Agency

Nuclear Weapons Effects Subtask SB209

Conducted for U. S. Army Engineer Waterways Experiment Station, Vicksburg, Mississippi

Under Contract No. DACA39-69-C-0022

By Paul Weidlinger, Consulting Engineer, New York, New York

ARMY-MRC VICKSBURG, MISS

FOREWORD

The investigations leading to this report were conducted for the U. S. Army Engineer Waterways Experiment Station (WES) under sponsorship of the Defense Atomic Support Agency (DASA)* under Nuclear Weapons Effects subtask SB209, "Propagation of Ground Shock Through Earth Media."

The contract was monitored by Dr. G. Y. Baladi, Dr. J. S. Zelasko, and Mr. P. F. Hadala, Impulse Loads Section, Soil Dynamics Branch, under the general supervision of Mr. J. P. Sale, Chief, Soils Division, WES. COL Ernest D. Peixotto, CE, was the contracting officer. Director of the WES during conduct of this study and publication of this report was COL Peixotto; Technical Director was Mr. F. R. Brown.

---

* Now designated the Defense Nuclear Agency.

ABSTRACT

In recent years, the development of mathematical models for the study of ground shock effects in soil and/or rock media has made important progress. Currently, three basic types of advanced models have been studied: (a) elastic-ideally plastic models, (b) variable moduli models, and (c) elastic-nonideally plastic capped models. This paper is the first part of an investigation which is aimed at studying the behavior of the different types of models in ground shock problems.

The ground shock response in the superseismic range of a one megaton air burst on a homogeneous half-space of a soil is considered. Each of the three types of models was fitted to laboratory test data and calculations were made for each case. Generally, the results from all three models are comparable only when the stress paths in uniaxial strain are comparable for complete load-unload cycles. When this is not so, major differences occur in the lateral motions and stresses.

INFLUENCE OF CONSTITUTIVE MODELS ON GROUND MOTION PREDICTIONS

Table of Contents

LIST OF SYMBOLS*)

a_1 , a_2 , a_3	Coefficients in Eqs. (2) and (7).
A, B, C	Constants defined by Eq. (16).
c_{P_0} , c_{S_0} , $c_{P_{max}}$	Initial P and S wave velocity, maximum wave velocity.
D	Constant defined by Eq. (18).
E	Young's modulus.
e_{ij}	Strain deviator.
F	Measure of state of stress defined by Eq. (13).
F(L)	Semi-minor axis of elliptical soil cap, Fig. (4).
F_{max}	Maximum previous value of F.
f	Yield condition.
f_1	Ideally-plastic yield condition in cap model.
f_2	Hardening yield condition or cap.
G	Shear modulus.
G_{LD} , G_{UN} , G_{RE}	Shear modulus in loading, unloading, reloading.
G_0	Initial shear modulus.
G_{0U} , G_1 , G_{1U}	Constants in expressions for variable G, Eqs. (11).
$G_{max\ U}$	Maximum value of G_{UN} .
J_1	First invariant of stress tensor.
J_2'	Second invariant of stress deviator.
K	Bulk modulus.
K_{UN}	Bulk modulus in unloading.
K_0	Initial bulk modulus.
K_{0U} , K_{1U} , K_{max}	Constants in expressions for K_{UN} .

*) Additional symbols are defined as they occur in the text.

k	Cohesion.
k_{eff}	Effective shear strength at high pressure defined by Eqs. (1).
L	Coordinate defining center of ellipse, Fig. (4).
M	Constrained modulus.
n	Integer or constant in Eq. (12).
p	Pressure = $J_1/3$.
p_c	Critical or transition pressure in Eqs. (1) and (11).
p_m	Transition pressure in Eqs. (3) and (8).
R	Range, or ratio between axes of elliptical cap, Fig. (4).
s_{ij}	Deviatoric stress tensor.
s_z	Axial stress deviator.
u, w	Horizontal, vertical velocity.
X	Value of J_1 at intersection of cap and J_1-axis, Fig. (4).
z	Depth.
α	Coefficient in yield condition, Eqs. (1).
$\bar{\gamma}$, γ_1, γ_2	Constants in expression for G_{LD}.
$\bar{\gamma}_U$, γ_{1U}, γ_{2U}	Constants in expression for G_{UN}.
δ_H, δ_V	Horizontal, vertical displacement.
ε_{ij}	Strain tensor.
ε_{kk}	Volumetric strain.
ε^P	Plastic volumetric strain, ε^P_{kk}.
ν, ν_0	Poisson's ratio, initial Poisson's ratio.
ν_{LD}, ν_{UN}	Poisson's ratio in loading, unloading.
ρ	Density.
σ_{ij}	Stress tensor.
σ_r, σ_z	Radial, vertical stress.

I INTRODUCTION.

In recent years, the development of mathematical models for the study of ground shock effects in soil and/or rock media has made important progress, Refs. [1], [2]. Currently, three basic types of advanced models have been studied: (a) elastic-ideally plastic models; (b) variable moduli models; and (c) elastic-nonideally plastic capped models. A detailed summary of the advantages and disadvantages of each type of model is given in Refs. [1], [2]. Table I of Refs. [1], [2] is repeated in this report for convenience.

The present paper is the first part of an investigation aimed at studying the behavior of the different types of models in ground shock problems of interest. The study involves fitting a mathematical model of each type to the same set of experimental data and then using these models to analyze a series of ground shock problems. The aim of the investigation is to evaluate the influence of the various constitutive models on ground motion calculations, and to explain any differences that might arise. It is intended to expand this study to include comparative calculations of field tests and eventually to make recommendations on the use of the models for a wide range of pressure levels, geometries (layering) and soil properties.

This paper considers a one megaton (1 MT) air burst on a homogeneous half-space, Fig. (1), of a soil material, namely McCormick Ranch sand. This material was chosen because it was

one of the very few soil materials for which a large amount of laboratory data was available. Material model fits for the two more sophisticated results, i.e., the variable moduli model, Ref. [3], and the soil cap model, Ref. [4], were already available from our previous studies. The elastic-ideally plastic fit was developed specifically for the present study.

Results are monitored for a number of surface pressure levels in the high superseismic region (Mach = 8) and a comparison of the ground shock results obtained with all three models is made. As might be expected, the results indicate the great importance of modeling correctly the stress path in unloading in uniaxial strain. It should be noted that in the past, stress path information from the uniaxial strain test was usually missing from available experimental results. One purpose of this paper will be to emphasize the importance of making such information available to the model developer by means of a uniaxial strain null test. Important studies towards obtaining reliable null test data are currently in progress at the Waterways Experiment Station.

The soil selected for modeling was McCormick Ranch sand because this was one of the few materials for which <u>almost</u> all of the laboratory data from the standard tests was available. This data included: (a) uniaxial strain test results for longitudinal stress versus longitudinal strain over a load-unload cycle (however, <u>no lateral stress versus longitudinal stress data</u> and hence, no stress path was

available); (b) triaxial compression test results including stress difference versus strain and strain difference curves in cyclic loading and stress difference at failure for each test; and (c) proportional loading test axial stress versus axial strain results. The material is characterized by a considerable amount of hysteresis in a load-unload cycle in either uniaxial strain or triaxial compression.

The study presented here is limited to the superseismic region of the material. Generally, the results from all three models are comparable when the stress paths in uniaxial strain are comparable for complete load-unload cycles. When this is not so, major differences can be found in the lateral motions and stresses, although the vertical motions and stresses are still governed primarily by the stress-strain curve for the uniaxial strain test and hence, are only slightly affected. Consequently, particular attention is paid to the evaluation of these lateral (horizontal) motions in this paper.

This first study does not include layering effects. Some preliminary results for the case of a rigid bottom at a given depth are also discussed. The study is currently being extended to other geometries (layered materials), ranges (transseismic and subseismic) and materials of interest.

II MATERIAL MODELS.

McCormick Ranch sand was used previously to illustrate the fitting of both the variable moduli and soil cap models to a real material. Each of these fits was done by different investigators, independently, using the same rather extensive set of laboratory data. The descriptions of these fits, including comparisons with experimental data, are well documented in previous reports, Ref. [3], for the variable moduli, and Ref. [4] for the soil cap model. The minor differences in the fits to the various test curves are not significant. The important thing to note is that each model represented a good fit to the available laboratory data. Many of the differences that occur are attributable to differences in procedure and philosophy of the individual modeler. For example, the constant unloading (elastic) bulk modulus in the cap model is not necessary to the cap model formulation. A variable unloading bulk modulus, such as is used in the variable moduli approach, could easily be incorporated into the cap model. The elastic-ideally plastic fit was made specifically for this comparison. It cannot really be considered to be completely independent of the variable moduli fit, since it was made by the same person after the variable moduli fit had already been completed. In fact, certain relations such as the unloading bulk modulus and the failure envelope*) are identical in these two models.

---

*) The "failure envelope" for the variable moduli material can be defined as the surface $f(J_2', p) = 0$ such that $G_{LD} = 0$.

McCormick Ranch sand is characterized by a large amount of hysteresis in a load-unload cycle in uniaxial strain, see Fig. (2). Also illustrated in Fig. (2) are stress-strain relations in uniaxial strain computed with the three models. Except for the tail at low stress in unloading both the variable moduli and cap fits follow the experimental curve extremely well. The elastic-ideally plastic fit which was used deviates somewhat more. The reader is referred to Refs. [3] and [4] (or more briefly to Sections IV and V of Refs. [1], [2]) for additional laboratory data as well as the details of the fits. A brief description of the three types of models follows.

(A) Elastic-Ideally Plastic Model.

Model of this type are currently being used for most ground shock calculations. They have been described in detail in several papers, Refs. [1], [2], [5], [6], and only a summary is given here.

The model is characterized by a yield condition of the type, Fig. (3)

$$\begin{aligned} \sqrt{J_2'} &= k + 3\alpha p\left(1 - \frac{p}{2p_c}\right) && p \le p_c \\ &= k + \frac{3}{2}\alpha p_c = k_{eff} && p \ge p_c \end{aligned} \qquad (1)$$

For this soil, a nonassociated flow rule of a von Mises type is used to remove "dilatancy" effects from yielding. This leads to a unique pressure-volumetric strain relation on

initial loading. This pressure, which is given by

$$p_{max}(\varepsilon_{kk}) = \sum_{n=1}^{3} a_n \varepsilon_{kk} \tag{2}$$

is the maximum pressure possible at a given volumetric strain. For unloading, and subsequent reloading up to the previously reached maximum pressure on the virgin loading curve, a variable bulk modulus of the form

$$\begin{aligned} K_{UN}(p) &= K_{0U} + K_{1U}p && p \leq p_m \\ &= K_{max} && p \geq p_m \end{aligned} \tag{3}$$

is used. In the model, Poisson's ratio is assumed to be piecewise constant, i.e.,

$$\begin{aligned} \nu &= \nu_{LD} = \text{Constant} \quad \text{(Loading)} \\ \nu &= \nu_{UN} = \text{Constant} \quad \text{(Unloading and Reloading)} \end{aligned} \tag{4}$$

where the choice is based upon which pressure-volume relation is used. In the calculations, a tension cutoff was used

$$p \geq 0 \qquad \text{(No mean tension)} \tag{5}$$

Two models were used in the calculations: (1) one in which the same constant value of ν was used in both loading and unloading and (2) one in which different constant values of ν_{LD} and ν_{UN} were used for loading and unloading, respectively. A summary of the material constants used in the elastic-

ideally plastic fit*) is given in Table II.

As is usual in such models, the stress-strain curve in uniaxial strain was modeled over a full load-unload cycle and the yield condition was fitted to the failure envelope from the triaxial compression tests. The stress difference-strain curves for the triaxial tests could not be modeled once yielding started; this is a limitation on and a characteristic of such elastic-ideally plastic models.

(B) Variable Moduli Model.

Models of this type have been discussed in detail in Refs. [1], [2], [3], [7], [8], and some two dimensional calculations have been made, Ref. [9], for comparison with a series of analytical solutions, Refs. [10], [11]. In this model, both the bulk and shear moduli are functions of the stress and/or strain invariants and no explicit yield condition is specified. The mathematical description is given in terms of the incremental stress-strain relations

$$\dot{p} = K\,\dot{\epsilon}_{kk} \qquad \text{(a)}$$

$$\dot{s}_{ij} = 2G\,\dot{e}_{ij} \qquad \text{(b)} \qquad (6)$$

It should be noted that the separation of the constitutive relations into a deviatoric and a volumetric part, while

*) It should be noted that not all of the constants in Table II are independent.

convenient, precludes dilatancy in the material. Consequently, this model is not intended to represent materials such as rock when significant dilatancy may be observed.

The pressure-volume relations are given by

$$p_{max}(\varepsilon_{kk}) = \sum_{n=1}^{3} a_n \varepsilon_{kk}^n \qquad \text{Initial loading} \tag{7}$$

$$\left.\begin{aligned} K_{UN}(p) &= K_{0U} + K_{1U}p \qquad p \leq p_m \\ &= K_{max} \qquad\qquad p \geq p_m \end{aligned}\right\} \tag{8}$$

$$p \geq 0 \qquad \text{Tension Cutoff} \tag{9}$$

The quantity $K_{UN}(p)$ is used for both unloading and reloading regimes.

The deviatoric stress-strain behavior is given by Eq. (6b) where the shear modulus G is defined separately in loading, unloading and reloading as

$$\left.\begin{aligned} G &= G_{LD}(p, \sqrt{J_2'}) \quad \text{when } F = F_{max} \text{ and } \dot{J}_2' > 0 \qquad \text{(a)} \\ G &= G_{UN}(p, \sqrt{J_2'}) \quad \text{when } \dot{J}_2' \leq 0 \qquad\qquad\qquad \text{(b)} \\ G &= G_{RE}(p, \sqrt{J_2'}) \quad \text{when } F < F_{max} \text{ and } \dot{J}_2' > 0 \qquad \text{(c)} \end{aligned}\right\} \tag{10}$$

where the quantities G_{LD} , G_{UN} are given by

$$\left.\begin{aligned} G_{LD}(p, \sqrt{J_2'}) &= G_0 + \bar{\gamma}\sqrt{J_2'} + \gamma_1 p + \gamma_2 p^2 \qquad p \leq p_c \\ &= G_1 + \bar{\gamma}\sqrt{J_2'} \qquad\qquad\qquad\qquad p \geq p_c \\ G_{UN}(p, \sqrt{J_2'}) &= G_{0U} + \bar{\gamma}_U\sqrt{J_2'} + \gamma_{1U} p + \gamma_{2U} p^2 \qquad p \leq p_c \\ &= G_{1U} + \bar{\gamma}_U\sqrt{J_2'} \qquad\qquad\qquad\qquad p \geq p_c \end{aligned}\right\} \tag{11}$$

During reloading (in shear) defined by Eq. (10c), the shear modulus G_{RE} is taken as the linear combination of G_{LD} and G_{UN} :

$$G_{RE}(p, \sqrt{J_2'}) = (\frac{F}{F_{max}})^n \, G_{LD}(p, \sqrt{J_2'}) + [1 - (\frac{F}{F_{max}})^n] \, G_{UN}(p, \sqrt{J_2'}) \tag{12}$$

where n is a constant. The ratio $\frac{F}{F_{max}}$ is a measure of the current state of stress F, defined by

$$F(p, \sqrt{J_2'}) = 1 - \frac{G_{LD}(p, \sqrt{J_2'})}{G_{LD}(p, 0)} \tag{13}$$

to the maximum previous state, F_{max} . The function F is restricted to the range

$$0 \leq F \leq 1 \tag{14}$$

so that

$$G_{LD}(p, \sqrt{J_2'}) \leq G_{RE}(p, \sqrt{J_2'}) \leq G_{UN}(p, \sqrt{J_2'}) \tag{15}$$

The various constants*) used in this fit are given in Table III. Detailed comparisons of this fit**) to laboratory data for McCormick Ranch sand are presented in Ref. [3] and in Section IV of Refs. [1], [2].

---

*) As in the previous case, not all of these constants are independent.

**) The current variable moduli fit is a slight modification of the fit referred to as "Uniax-Triax II" in Ref. [3]. The unloading shear parameters G_{0U} , γ_{1U} (and γ_{2U}) are somewhat altered. The reloading parameter n, not given elsewhere, was chosen as 4 somewhat arbitrarily.

The theory of variable moduli models is rigorously correct for cases of proportional loading in shear. Continuity problems may arise for complicated stress paths in which neutral loading in shear occurs. One purpose of this study is to ascertain the behavior of the model in ground shock problems which although not a case of proportional loading in shear, would not be expected to exhibit significant neutral loading.

(C) Soil Cap Model.

This model represents the latest step in the development of soil and rock models, Refs. [1], [2], [4], [12]. It is characterized by the specification of elastic-nonideally plastic constitutive relations with a capped yield surface. A yield surface which combines both ideal plasticity and strain-hardening is postulated and an associated plastic flow rule is used. The model is capable of predicting observed laboratory data from all available tests and at the same time satisfies the most restrictive theoretical requirements of continuity, stability and uniqueness.

For soil, the yield conditions, Fig. (4), consist of an ultimate failure condition of a form slightly different*) than Eqs. (1)

$$f_1(J_1 , \sqrt{J_2'}) = \sqrt{J_2'} - [A - C \exp(-BJ_1)] = 0 \qquad (16)$$

where $J_1 = 3p$, and an interval strain-hardening cap which

*) This difference is another example of difference in philosophy of the two modelers referred to earlier. Equations (1) could have been used here just as well.

"expands" or "contracts" as the plastic volumetric strain increases or decreases, respectively. In the present fit to McCormick Ranch sand, an elliptical cap, See Fig. (4), of the form

$$f_2(J_1 , \sqrt{J_2'} , \varepsilon^P) = (J_1 - L)^2 + (R\sqrt{J_2'})^2 - (X - L)^2 = 0 \quad (17)$$

was used, where R is the constant ratio of the major to the minor axis, and where $L(\varepsilon^P)$ and $X(\varepsilon^P)$ are, respectively, the values of J_1 at the center of the ellipse and at the intersection of the cap with the J_1 axis. The function $X(\varepsilon^P)$ relating the position of the cap to the plastic strain is given by

$$X(\varepsilon^P) = -[\ell n(1 - \varepsilon^P/W)]/D \quad (18)$$

where W and D are constants.

Within the current yield surface the material behaves elastically with a constant shear modulus G. The elastic bulk modulus K can be a function of pressure without raising any theoretical objections. However, for the present fit to McCormick Ranch sand a constant bulk modulus was considered sufficient. Consequently, the value of Poisson's ratio within the yield surface also is a constant. The values of the constants used in the current fit are given in Table IV.

All theoretical requirements for continuity, stability and uniqueness are satisfied by the cap model. It should be noted that since the movement of the cap is controlled by the increase or decrease in the plastic volumetric strain,

strain-hardening can be reversed in this model and this mechanism leads to an effective control on dilatancy*), which can be kept quite small (effectively zero) as required for a soil model. The reader is referred to Ref. [4] and Section V of Refs. [1], [2], for the details of the soil cap model as well as comprehensive comparisons of the fit of the theoretical model to the laboratory test data.

No attempts were made to make the models similar and hence, each fit represents what a qualified investigator might come up with independently, given the laboratory data available. This aspect of the model fitting will be quite important in the discussion of the numerical results in Section III.

*) The use of a pressure dependent yield condition with an associated flow rule necessarily leads to "dilatancy", an inelastic volume change due to yielding.

III COMPUTATIONAL RESULTS AND DISCUSSION.

For comparative purposes, the models were each separately run, using the LAYER Code, for the case of a 1 MT, 1500 ft height of burst explosion on a half-space of the McCormick Ranch sand material. In the computations, the surface loading (Brode H-1 loading, Ref. [13]), the number of grid points in the horizontal and vertical directions, the horizontal and vertical spacing of the grid points (20 ft by 20 ft) and the treatment of the grid boundaries were identical for all three runs. The left boundary included the origin, R = 0, the right boundary assumed the velocities to be continuous across the boundary while the bottom boundary was of the transmitting type, Refs. [14], [15], so that a half-space was effectively simulated. All runs used an iterative stress boundary condition on the surface, z = 0, Ref. [15], so that the applied surface stress and the constitutive relations were both satisfied. Of course, different constitutive relations were applied for each run.

Since the unloading bulk modulus K_{UN} in both the variable moduli and the elastic-ideally plastic models varied with pressure, the maximum unloading P wave velocities at high pressures (4157 ft/sec and 4368 ft/sec, respectively) were considerably greater than the constant (elastic) unloading P wave speed of 2068 ft/sec for the cap model. Consequently, while the run for the cap model could be made with 6 ms time steps, Courant-Friedrichs-Lewy stability required the time step for the other two runs to be only 3 ms.

For the highly superseismic range being studied here, the vertical displacements were considerably larger than the horizontal displacements. Detailed results are presented for the displacements over a substantial portion of the superseismic region and in particular at the 1000 psi (R = 1660 ft) and 500 psi (R = 2060 ft) surface pressure levels.

Figure (5) shows a plot of the horizontal displacement versus range curves for all three models at time t = 1167 ms for a near surface point (depth z = 30 ft). It is seen that while the horizontal displacements from the variable moduli and cap models are comparable (within 20%), the elastic-ideally plastic model gives significantly smaller horizontal displacements, sometimes by a factor of as much as two (when compared with the variable moduli results). On the other hand, a similar plot of vertical displacement versus range gives comparative results which are virtually indistinguishable for all three models.

To investigate the reason for the differences in the highly sensitive horizontal displacements, the time histories of the horizontal velocities at the 500 psi contour are shown in Fig. (6) for the cap and the elastic-ideally plastic models. It is seen that while at early times these histories are quite comparable, the signal from the cap model computations remains at a considerably higher level than that from the elastic-ideally plastic model computations at later times; this results in a significantly larger horizontal displacement for the cap model. To further understand these differences, the time plots for the radial stress σ_r are shown in Fig. (7)

for both models. Again it is seen that for very early times the signals are comparable but that at later times significantly larger radial stresses are given by the cap model.

The reason for these differences is best seen by considering the stress paths of the three models in a uniaxial strain configuration for a complete load-unload cycle. For the present highly superseismic case (Mach number ≃ 8) the actual state of stress in the material can be considered similar to that in a uniaxial strain test.

The stress path in uniaxial strain, where there is a single independent stress deviator, is illustrated in Fig. (8) as a plot of the axial stress deviator s_z versus the mean stress or pressure p. In this (s_z , p) space, points on a line with a slope of -1 correspond to a constant value of σ_z , while those on a line with a slope of +2 correspond to a constant value of σ_r . The loci $\sigma_z = 0$ and $\sigma_r = 0$ are shown in Fig. (8). Points on lines parallel to $\sigma_z = 0$ ($\sigma_r = 0$) but to the right correspond to larger values of σ_z (σ_r). The failure envelope, Eqs. (1) or Eq. (16), appears on the plot as a pair of curves symmetric with respect to the p axis since $\sqrt{J_2'} = \pm \frac{\sqrt{3}}{2} s_z$ for this geometry.

The stress paths for all three models start at the origin (stress free state) and load up to an axial stress $\sigma_z = 400$ psi. The cap and the variable moduli curves are very close to one another, starting almost tangent to $\sigma_r = 0$ (which would correspond to $\nu_0 = 0$), and bending over as they approach the failure surface. The elastic-ideally plastic model, with a

constant Poisson's ratio, loads along the straight line (2) which falls short of intersecting the failure envelope. The unloading path for this model differs even more drastically from those of the other two models.

The curve marked (2) is also the unloading stress path for the original elastic-ideally plastic model which utilized the same constant Poisson's ratio $\nu = 0.30$ in both loading and unloading. It is seen that the material loads along a straight line to $\sigma_z = 400$ psi and unloads back down the same line to $\sigma_z = 0$. At the completion of unloading, the radial stress σ_r is equal to zero.

The dotted curve shows the stress path in loading and unloading for the cap model. The loading path is a curve up to the 400 psi level, and a straight line for unloading to the zero level at the point B. It is important to note, however, that the cap model (which is linearly elastic in unloading) unloads with a constant value of Poisson's ratio $\nu_{UN} = 0.25$ and that when the $\sigma_z = 0$ line is reached at point B, a residual radial stress σ_r of 75 psi is maintained in the material.

The variable moduli model, represented by the thick black line in the figure, loads along a curve to $\sigma_z = 400$ psi and then unloads along a different curve to the $\sigma_z = 0$ line at the point C where a level of residual radial stress of $\sigma_r = 44$ psi is noted. It is now apparent as to why the radial stress from the ground shock calculations for the cap and the

elastic-ideally plastic models differed, since the former unloads quite differently from the latter (i.e., it maintains a residual radial stress). This difference in the stress path for the three models, and in particular, the major differences in the unloading stress path between the cap and the elastic-ideally plastic models are responsible for the large differences in the horizontal displacements which were shown in Fig. (5) at the 500 psi pressure contour. The loading stress paths and more significantly, the unloading stress paths for the cap and the variable moduli model are quite similar, thus leading to radial stresses and velocities which are similar and hence, more comparable horizontal displacements, as shown in Fig. (5). The elastic-ideally plastic model has a quite different stress path history and hence, gives significantly different (in this case lower) radial stresses, velocities and displacements.

To test this marked dependence of the horizontal quantities on the stress paths in loading, and more particularly unloading, a second calculation was run with an elastic-ideally plastic model in which the Poisson's ratio in unloading was matched with that of the cap model, i.e., $\nu_{UN} = 0.25$. The loading stress path for this case is again given by the straight line (2) in Fig. (8), but the unloading curve is now parallel to that of the cap model and is shown by the straight line (1). It is noted that upon complete unloading to $\sigma_z = 0$, a residual radial stress $\sigma_r = 38$ psi [Point A in Fig. (8)] is obtained. It will be shown later in this section that the horizontal displacements

for this revised elastic-ideally plastic model (in which the unloading stress path is more comparable to those for the cap and the variable moduli models) are much closer to the corresponding values for the cap and the variable moduli models.

The importance of having models which give similar stress paths in loading-unloading cycles is further illustrated by considering a loading to the higher stress level σ_z = 1000 psi, as shown in Fig. (9). In this case, the loading was sufficiently high for the elastic-ideally plastic model to plasticize. The elastic-ideally plastic model loads along the straight line, yields at the intersection of this line with the yield surface and continues loading along the yield surface to the σ_z = 1000 psi line. It then unloads linearly along line 2 (when ν_{UN} = 0.30 is used) or line 1 (when ν_{UN} = 0.25 is used) until it replasticizes on the other side of the yield surface and then continues along the lower yield surface until the final point at σ_z = 0 is reached. The cap model loads along the dotted curve to the σ_z = 1000 psi line, and then unloads along the straight dotted line until the line meets the lower portion of the yield surface and replasticization occurs. It then unloads along the lower yield surface to the final point at σ_z = 0. The variable moduli model loads along the heavy black curve and unloads along the heavy black curve until once again the final point at σ_z = 0 is reached.

For this case of loading to a high stress level, i.e., a level in which the yield surface plays a significant role in the elastic-ideally plastic model, all three models have a very

similar loading stress path. However, the stress paths in unloading are still different, but not nearly as different as they were for the previous case, Fig. (8). One might therefore expect that the computed horizontal displacements at the 1000 psi level for the elastic-ideally plastic model with $\nu_{UN} = 0.3$, the cap model and the variable moduli model would agree somewhat better than those for the case of loading to 500 psi. This is in fact borne out in Fig. (5). For the case of the elastic-ideally plastic model with $\nu_{UN} = 0.25$ (equal to ν_{UN} for the cap model), the stress path histories are quite similar for all three models and much closer agreement would be expected for the horizontal displacements from the ground shock calculations, as shown in the curves which follow.

Figures (10)-(20) show comparative results for the calculations with the elastic-ideally plastic model with $\nu_{UN} = 0.25$, the cap model and the variable moduli model. It is seen that generally, excellent agreement is obtained from the three models. Figure (10) shows the curve of vertical displacement versus range for all three models. It is seen that the results are practically indistinguishable. If the uniaxial strain test stress-strain relations for the three models were identical over the entire stress range shown in Fig. (10), the three curves in the figure would essentially coincide. While the curves produced by the variable moduli and elastic-ideally plastic models almost coincide, the vertical displacements computed with the cap model are slightly larger at both the high and low stress levels. The three curves

do coincide at about the 1000 psi overpressure level since the models were all fit using the experimental uniaxial strain test to 1000 psi, Fig. (2). No attempt was made to make the models do more than behave reasonably when extrapolated to stress levels significantly above 1000 psi, since uniaxial strain data was not available. The unloading bulk moduli for the variable moduli and elastic-ideally plastic models are identical*), while for peak vertical stresses less than about 370 psi (p = 240 psi) the cap unloading bulk modulus is stiffer than that of the other models and consequently, the vertical displacement is larger.

Figure (11) shows the variation with range of the maximum horizontal displacements computed with the three models. It is seen that the peak horizontal displacements are fairly close over the entire range, with the maximum difference being on the order of 20%. The results for the elastic-ideally plastic model are consistently lower than those for the other two models. The variable moduli and cap results agree extremely well over a wide range of surface overpressures.

Figure (12) shows the attenuation of peak vertical and radial stresses with depth below the (nominally) 500 psi surface pressure contour. The computed vertical stress attenuations for the three models agree extremely well for depths less than z ≃ 150 feet. Below that level, the additional hysteresis in the cap model, due to the stiffer unloading bulk

*) These two models were fit by the same investigator.

modulus at low stresses, causes the additional attenuation in the vertical stress for that model to be noticeable. Near the surface, where the peak vertical stresses agree, the peak computed radial stress is largest with the cap model, and smallest with the elastic-ideally plastic model. This result agrees with the uniaxial strain stress paths shown in Fig. (8). When the vertical stresses attenuate to less than 200 psi, the radial stress computed with the elastic-ideally plastic model is the largest, a result again suggested by Fig. (8).

Figure (13) shows the attenuation of the peak vertical and horizontal velocities with depth at the same 500 psi pressure contour. As was the case with the vertical stresses in Fig. (12), the peak vertical velocities computed with the variable moduli and elastic-ideally plastic models agree extremely well, reflecting the similarity in their uniaxial strain stress-strain relations. At sufficient depth the additional hysteresis in the cap model produces smaller vertical velocities, again following the pattern in Fig. (12). The peak horizontal velocities computed with the three models agree fairly well, at least to depths of $z \simeq 200$ ft. It should be noted that the horizontal velocities do not attenuate.

The attenuation in the peak vertical and horizontal displacements at the 500 psi pressure contour is shown in Fig. (14). In each case, the results are fairly close and the trends are similar for all three computations. The elastic-ideally plastic model consistently predicts the smallest horizontal displacement. It should again be noted that the horizontal displacements do not attenuate.

It is also of interest to compare time histories of displacements, velocities and stresses at points in the medium. Figure (15) shows vertical displacements versus time at a near surface point below the 500 psi surface pressure load (z = 30 ft, R = 2070 ft). The results for all three cases are quite comparable. The remarkable agreement between the variable moduli and elastic-ideally plastic models may again be attributed to the similarity in their uniaxial strain stress-strain relations. Figure (16) shows horizontal displacement versus time curves at the same point. It is seen that the time histories for the variable moduli and cap models are very close while that of the elastic-ideally plastic model with $\nu_{UN} = 0.25$ is quite similar but somewhat lower. The horizontal displacement versus time curve for the earlier elastic-ideally plastic model, $\nu_{UN} = 0.30$, is also shown. It is of interest to note the considerable change in the values of δ_H when ν_{UN} is changed from 0.30 to 0.25 in the elastic-ideally plastic model. What is significant here is not the change in the value of ν_{UN}, but rather the change that this engenders in the unloading stress path in the two models. In Fig. (8), line (1) is approximately halfway between line (2) (corresponding in $\nu_{UN} = 0.30$) and the cap unloading path. Similarly, the horizontal displacement computed with $\nu_{UN} = 0.25$ is about halfway between the cap curve and the $\nu_{UN} = 0.30$ curve. Again, the importance of modeling the correct stress paths in both loading and unloading in uniaxial strain is indicated.

Figures (17) and (18) show plots of vertical velocity and vertical stress versus time at the point in question. In each case, the comparable curves from the three models are very similar, in fact, they are almost identical at early times.

The time history of radial stress σ_r computed with all three models is shown in Fig. (19). Despite the numerical oscillations, the three curves are seen to follow distinct trends after the first few oscillations. The cap and variable moduli curves are close to one another and significantly above the elastic-ideally plastic results for about the first third of the elapsed time shown. Thereafter, the radial stress computed with the variable moduli model approaches that computed with the elastic-ideally plastic model. This behavior agrees with that shown in Fig. (8) where the variable moduli stress path on unloading starts close to the cap stress path and approaches, but is always to the right of, line (1). This constant referral to the stress path in uniaxial strain, while extremely useful, is not the whole story in the present two dimensional problem. From Fig. (18) it is seen that the vertical stress goes essentially to zero at about one second while the radial stress, Fig. (19), continues to vary at much later times.

Finally, the horizontal velocity time histories at the same point, computed with the three models, are shown in Fig. (20). The general character of each of the curves is similar and the cap and the variable moduli curves agree most closely. The numerical oscillations, particularly at late times,

seem to be smallest in the variable moduli curve. This result is anticipated by the fact that the variable moduli is the only model of the three which contains additional hysteresis for cyclic loading within the current yield surface.

As a first step towards extending the present study to a layered geometry, the transmitting bottom boundary in the present geometry, Fig. (1), was replaced by a rigid bottom boundary. This approximates the effect of an underlying layer of hard rock. All other parameters were unchanged, the elastic-ideally plastic calculation being made with $\nu_{UN} = 0.25$. Preliminary results from this series of runs are shown in Figs. (21) and (22).

The variation of peak vertical displacements with range and overpressure level is shown for the rigid bottom calculations with all three models in Fig. (21). The previous results from Fig. (10) are repeated here for comparison. As can be expected, the vertical displacements are reduced by the presence of the rigid bottom boundary. In addition, the calculations agree extremely well with each other, as was true of the earlier transmitting bottom calculations.

The variation of peak horizontal displacements, from the rigid bottom calculations, is shown in Fig. (22), superimposed upon the previous results of Fig. (11). The effect of the rigid bottom on horizontal displacements is not as easy to predict as in the vertical case. The horizontal displacements are increased at high pressure levels (as they would be in a fluid) and decreased at lower pressure levels where the reflected

shear wave becomes of some importance. The agreement between the results predicted with the various models is nowhere as good as it was previously and, in fact, there again appears to be a difference of a factor of two between the elastic-ideally plastic model calculation (with $\nu_{UN} = 0.25$) and the variable moduli model. The cap results generally fall in between the other two, but agree much more closely with those from the variable moduli calculation. The analogy to the simple uniaxial strain case, which was so useful previously, is less satisfactory in explaining the current results.

IV CONCLUSIONS AND RECOMMENDATIONS.

Some interesting conclusions can be drawn on the basis of this series of calculations on a relatively simple geometry. First, the material models when fitted to laboratory data gave comparable vertical results (displacements, velocities and stresses) in each case. For the radial quantities, however, comparable results can only be obtained when the stress paths in a loading-unloading cycle in uniaxial strain are also comparable.

The present simulated half-space problem, which is highly superseismic (Mach ≃ 8 at the 500 psi level), leads to states of stress which are very close to those in uniaxial strain. The maximum slope of the peak vertical displacement versus depth curve, Fig. (14), suggests that the maximum vertical strain near the surface (z = 30 ft) at the 500 psi overpressure level is about 3%*), while the slope at the corresponding point for the peak horizontal displacement versus range curve, Fig. (11), suggests a maximum radial strain of less than 0.1%**). It is thus seen that the state of strain is nearly uniaxial and that consequently, any model, even a one dimensional model, which closely matched the experimental uniaxial strain test stress-strain curve, Fig. (2), would give good results for

---

*) It should be noted that although this slope is a strain-like quantity, it is not a true strain since the peak displacements occur at different times.

**) The maximum hoop strain at this point is known, i.e., $\varepsilon_{\phi} = \frac{\delta_H}{R} = 0.06\%$.

vertical stresses, velocities and displacements. A one dimensional model, however, would of course give no information on the small (as compared to the vertical effects) but real horizontal velocities and displacements which occur in this two dimensional problem.

The radial stress, velocity and displacement quantities are quite sensitive to both the uniaxial strain test stress-strain curves and, in particular, to the stress path of the material in a load-unload cycle. The radial stress time history is largely governed by the vertical stress and the stress path of the material in uniaxial strain. The radial stress in turn affects the horizontal velocity and hence, the horizontal displacement. Consequently, the stress path of the material in a load-unload cycle plays a crucial role in the evaluation of the horizontal quantities.

It is seen from the results that the horizontal motion for all three models agreed fairly well, although the results for the elastic-ideally plastic model were smaller than those for the others. The fact that the three models agreed as well as they did suggests that for this problem, the elastic-ideally plastic model would be a reasonable approximation to the more sophisticated models, provided that the stress path over a uniaxial strain test load-unload cycle were also modeled. The approximation becomes even better at higher stress levels, where the applied stress is significantly higher than the deviatoric stresses.

The results point out the importance of having more complete laboratory data from the uniaxial strain laboratory tests available to the model fitter. While the vertical effects are primarily governed by the stress-strain curve for hysteretic materials of this type, it is imperative to model the stress path in a loading-unloading cycle for a good definition of the radial effects. This means that in addition to the usual longitudinal stress versus strain data from a uniaxial test, lateral stress versus longitudinal stress data from this test is also urgently required. For effects in the superseismic range, it must be concluded that such data must be an integral part of the model fitting procedures.

The preliminary results for the case of a rigid bottom were discussed in Section III. The vertical displacements agree as well as those for the simpler half-space problem. The horizontal displacements on the other hand do not agree nearly as well as those for the half-space problem. Once again, the elastic-ideally plastic model gives smaller horizontal displacements, sometimes by as much as a factor of two. Figure (22) serves as a warning as to the extent of the uncertainties which will exist in the prediction of horizontal motions for more complicated geometries.

On the basis of the present study, it is not possible to recommend a single model as being most appropriate for use in <u>all</u> ground shock calculations. For the simple half-space problem considered, all three models gave comparable results as long as the unloading stress paths were somewhat

similar. The cap model is the only one which satisfies all theoretical requirements and at the same time fits all available laboratory data. On the other hand, it is more difficult to fit than the variable moduli model which also fits all the laboratory data. The variable moduli model, however, is theoretically correct only for cases of proportional loading in shear. The elastic-ideally plastic model cannot fit all of the laboratory data. The use of a constant Poisson's ratio and a nonassociated flow rule in this model can each lead to theoretical difficulties. The computer time required in the calculations with the two advanced models (for the same number of time steps) is similar and less than twice that required for the elastic-ideally plastic model computations.

These studies are currently being extended to layered geometries and other materials. In addition, effects in the transseismic and possibly subseismic regions will also be considered, in an effort to arrive at specific model recommendations for a wide variety of problems of interest.

TABLE I - Summary - Advantages and Disadvantages of Each Model.

Advantages	Disadvantages
A. Elastic-Ideally Plastic	
Simplest to fit. Approximates most features of data. $G=C$, $G=C(p_{max})$ and associated flow rule theoretically correct.	May not fit all available data. Cannot match triaxial test. Other treatments of G can lead to possible paths of energy generation. For nonassociated flow rule no general uniqueness theorem.
B. Variable Moduli	
Best fit of data. Only model with repeated hysteresis within failure envelope. Ideal for finite element. Computationally simple. Relatively easy to fit.	Restricted to near proportional loading (in shear). For nonproportional loading paths no uniqueness theorem. Additional quantity F_m must be stored at each grid point.
C. Soil Cap Model	
Satisfies all rigorous theoretical requirements. Reasonably good fit of data.	Indirect approach needed to fit data. Relatively complicated.

TABLE II

Material Constants for Elastic-Ideally Plastic Model of McCormick Ranch Sand

Yield Condition	k	73.1 psi	Unloading Bulk Modulus	K_{0U}	32.0 ksi
	α	0.0983		K_{1U}	143.0
	p_c	1082 psi		K_{max}	300 ksi
	k_{eff}	232.6 psi		p_m	1.8741 ksi
Initial Loading	$a_1 \equiv K_0$	10.24 ksi	Poisson's Ratio	ν_{LD}	0.30
	a_2	-211.31 ksi		ν_{UN}	0.30/0.25
p_{max}	a_3	3323.9 ksi	Density	ρ	131.1 lb/ft^3
Initial Moduli	G_0	4.726 ksi	Wave Speeds	c_{P_0}	764.6 ft/sec
	M_0	16.542 ksi		c_{S_0}	408.7 ft/sec
	E_0	12.288 ksi		$c_{P_{max}}$	4138/4368 ft/sec

TABLE III

Material Constants for Variable Moduli Model of McCormick Ranch Sand

Density	ρ	131.1 lb/ft^3	Unloading Bulk Modulus	K_{0U}	32.0 ksi
Initial Loading p_{max}	$a_1 \equiv K_0$	5.83 ksi		K_{1U}	143.0
	a_2	13.333 ksi		K_{max}	300 ksi
	a_3	1111.1 ksi		p_m	1.8741 ksi
Loading Shear Modulus G_{LD}	G_0	8.0 ksi	Unloading Shear Modulus G_{UN}	G_{0U}	8.0 ksi
	$\bar{\gamma}$	-110.0		$\bar{\gamma}_U$	500
	γ_1	32.4		γ_{1U}	33.0
	γ_2	-15.0/ksi		γ_{2U}	-15.278/ksi
	G_1	25.496 ksi		G_{1U}	25.820 ksi
	p_c	1080 psi		$G_{max\ U}$	141.71 ksi
	k_{eff}	231.8 psi	G_{RE}	n	4
Initial Moduli	ν_0	0.0292	Wave Speeds	c_{P_0}	763.5 ft/sec
	M_0	16.497 ksi		c_{S_0}	531.7 ft/sec
	E_0	16.468 ksi		$c_{P_{max}}$	4157 ft/sec

TABLE IV

Material Constants for Cap Model of McCormick Ranch Sand

Failure Envelope	A = 250 psi B = 6.7×10^{-4} psi^{-1} C = 180 psi
Elastic Moduli	K = 66.7 ksi G = 40.0 ksi M = 120.0 ksi E = 100.0 ksi
Elastic Poisson's Ratio	ν = 0.25
Cap Parameters	R = 2.5 W = 0.066 D = 0.67 ksi^{-1}
Density	130.0 lb/ft^3

REFERENCES

[1] Nelson, I., Baron, M.L. and Sandler, I., "Mathematical Models for Geological Materials for Wave Propagation Studies", Proceedings of the 17th Sagamore Army Materials Research Conference on Shock Waves and Mechanical Properties of Solids, September 1970.

[2] Nelson, I., Baron, M.L. and Sandler, I., "Mathematical Model for Geological Materials for Wave Propagation Studies", Forthcoming Technical Report, Defense Atomic Support Agency, Paul Weidlinger, Consulting Engineer, April 1971.

[3] Nelson, I., "Investigation of Ground Shock Effects in Nonlinear Hysteretic Media - Report 2 - Modeling the Behavior of a Real Soil", Report S-68-1, Contract DACA39-67-C-0048, Paul Weidlinger, Consulting Engineer, U.S. Army Engineer Waterways Experiment Station, July 1970.

[4] DiMaggio, F.L. and Sandler, I., "Material Models for Soils", Report DASA-2521, Paul Weidlinger, Consulting Engineer, Defense Atomic Support Agency, April 1970.

[5] Baron, M.L., McCormick, J.M. and Nelson, I., "Investigation of Ground Shock Effects in Nonlinear Hysteretic Media", Computational Approaches in Applied Mechanics, American Society of Mechanical Engineers, June 1969.

[6] McCormick, J.M., Baron, M.L. and Nelson, I., "Studies on the Distant Plain 1A Event", Report DASA 2213, Paul Weidlinger, Consulting Engineer, Defense Atomic Support Agency, July 1968.

[7] Nelson, I. and Baron, M.L., "Application of Variable Moduli Models to Soil Behavior", Presented at Sixth National Congress of Applied Mechanics, Harvard University, June 1970. To be published in International Journal of Solids and Structures, 1970.

[8] Nelson, I. and Baron, M.L., "Investigation of Ground Shock Effects in Nonlinear Hysteretic Materials - Report 1 - Development of Mathematical Material Models", Report S-68-1, Contract DACA39-67-C-0048, Paul Weidlinger, Consulting Engineer, U.S. Army Engineer Waterways Experiment Station, March 1968.

[9] Matthews, A.T. and Baron, M.L., "Investigation of Ground Shock Effects in Nonlinear Hysteretic Media - Report 5 - Computer Code Computations and Comparisons with Theoretical Solutions for Variable Moduli Materials", Report S-68-1, Contract DACA39-67-C-0048, Paul Weidlinger, Consulting Engineer, U. S. Army Engineer Waterways Experiment Station, August 1971.

[10] Matthews, A.T., Sandler, I. and Bleich, H.H., "Investigation of Ground Shock Effects in Nonlinear Hysteretic Media - Report 4 - Effect of a Step Load Moving with Constant Superseismic Velocity on a Half-Space of a Variable Modulus Material", Report S-68-1, Contract DACA39-67-C-0048, Paul Weidlinger, Consulting Engineer, U.S. Army Engineer Waterways Experiment Station, March 1970.

[11] Matthews, A.T. and Bleich, H.H. "Investigation of Ground Shock Effects in Nonlinear Hysteretic Media - Report 3 - Note on the Plane Waves of Pressure and Shear in a Half-Space of Hysteretic Material", Report S-68-1, Contract DACA39-67-C-0048, Paul Weidlinger, Consulting Engineer, U.S. Army Engineer Waterways Experiment Station, January 1969.

[12] Sandler, I. and DiMaggio, F.L., "Material Model for Rocks", Report DASA 2595, Paul Weidlinger, Consulting Engineer, Defense Atomic Support Agency, October 1970.

[13] Brode, H.L., "Height of Burst Effects at High Overpressures", The RAND Corporation, DASA 2506, Report RM-6301-DASA, July 1970.

[14] Lysmer, J.L. and Kuhlmeyer, R.L., "Finite Dynamic Model for Infinite Media", Journal Eng. Mech. Div., A.S.C.E., Vol. 95, No. EM4, August 1969.

[15] Matthews, A. T., "Effects of Transmitting Boundaries in Ground Shock Computations", Report S-71-8, Contract DACA39-70-C-0016, Paul Weidlinger, Consulting Engineer, U. S. Army Engineer Waterways Experiment Station, September 1971.

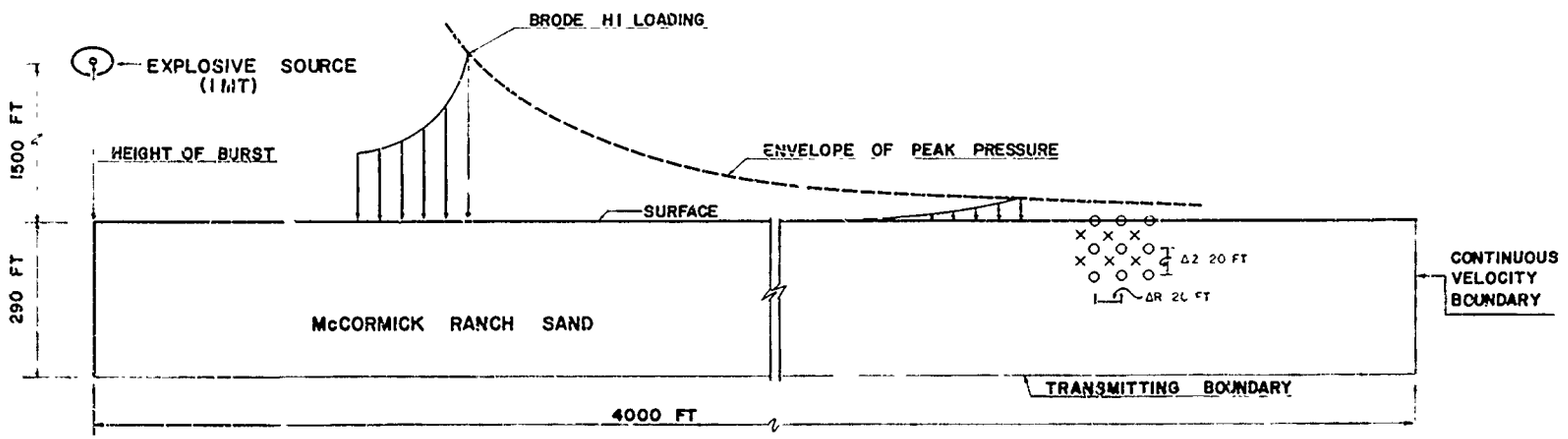

FIG. 1 GEOMETRY OF PROBLEM

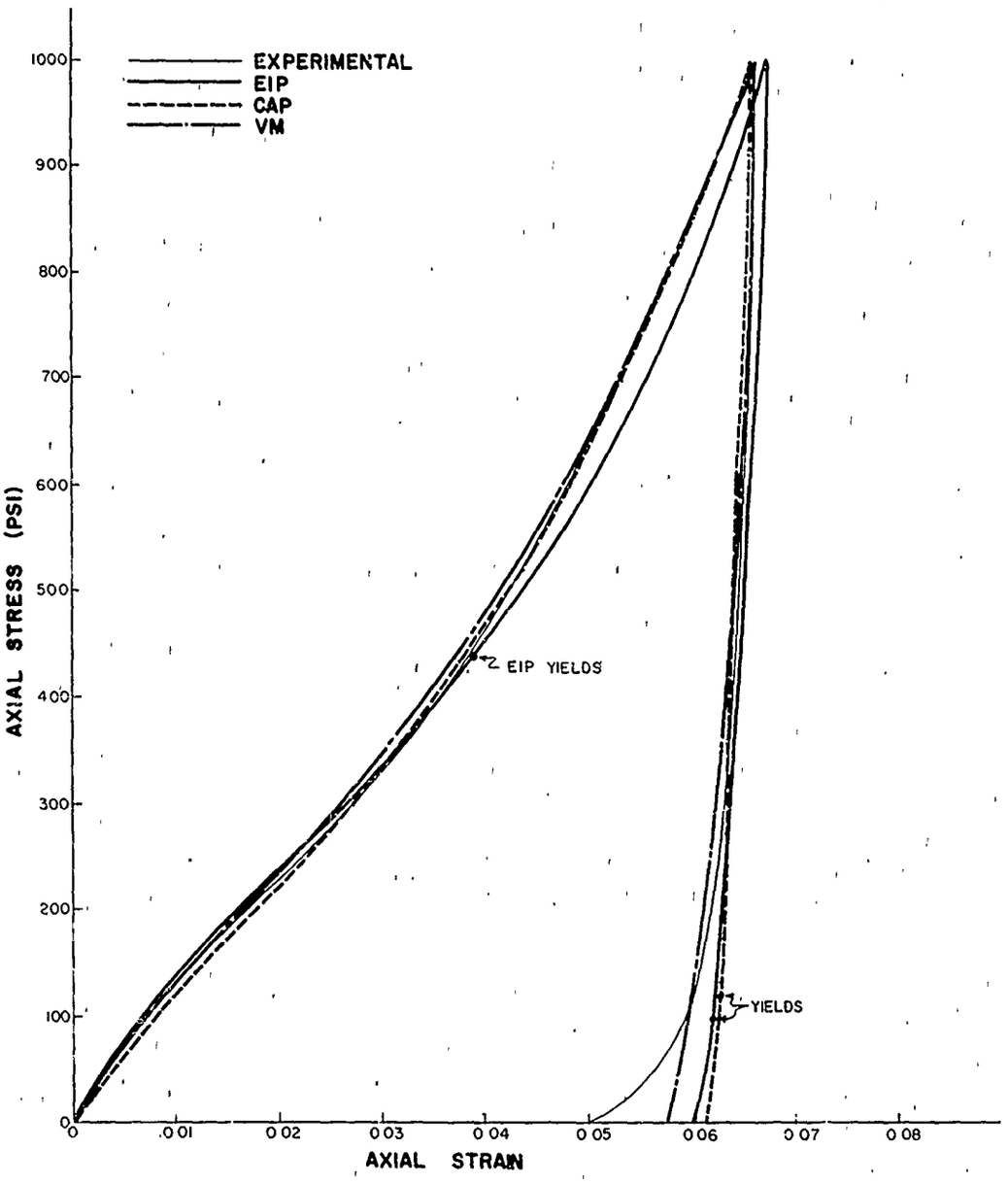

FIG. 2 UNIAXIAL STRAIN TEST FOR McCORMICK RANCH SAND COMPARISON OF THE THREE MODELS WITH EXPERIMENTAL DATA

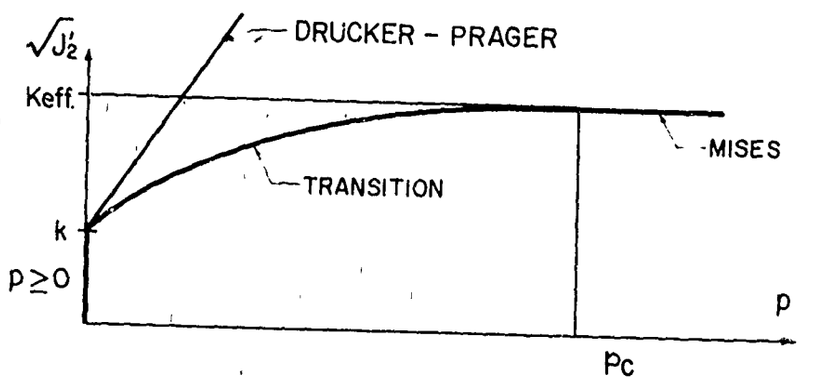

FIG. 3 YIELD CONDITION

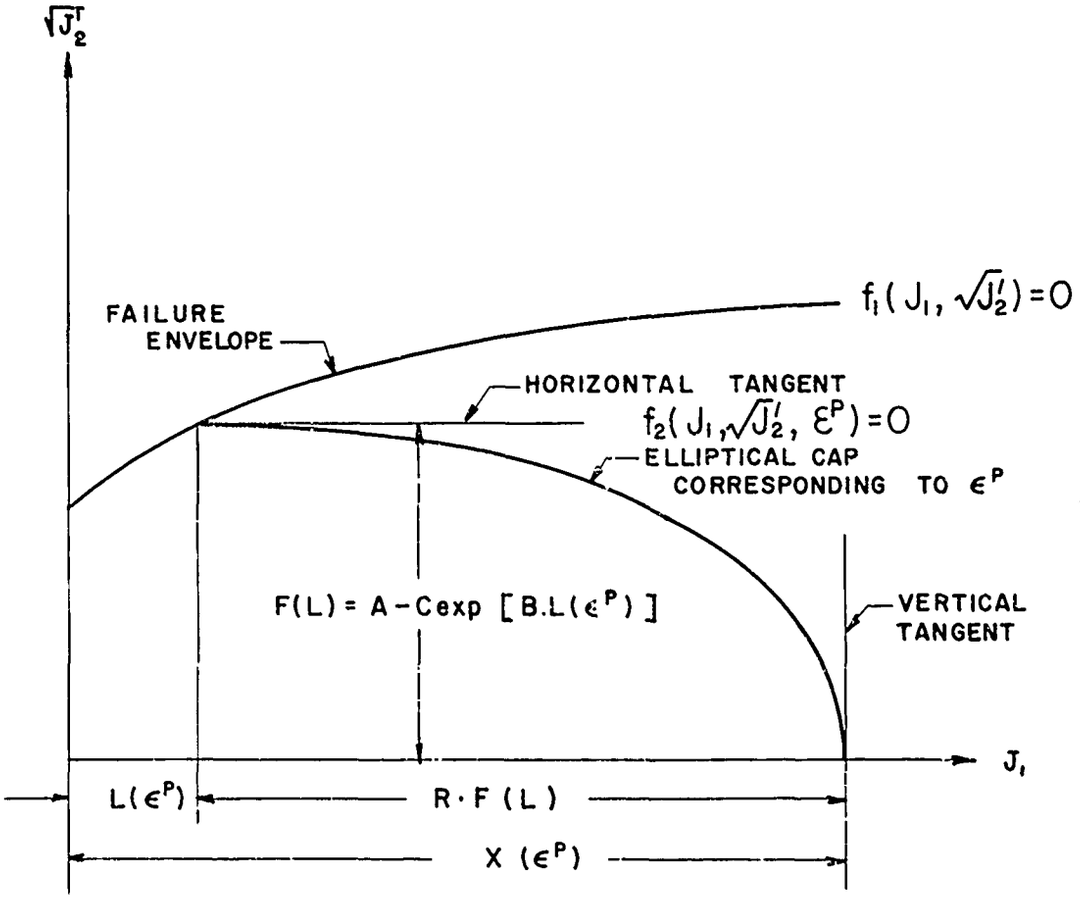

FIG. 4 DETAIL OF SOIL CAP

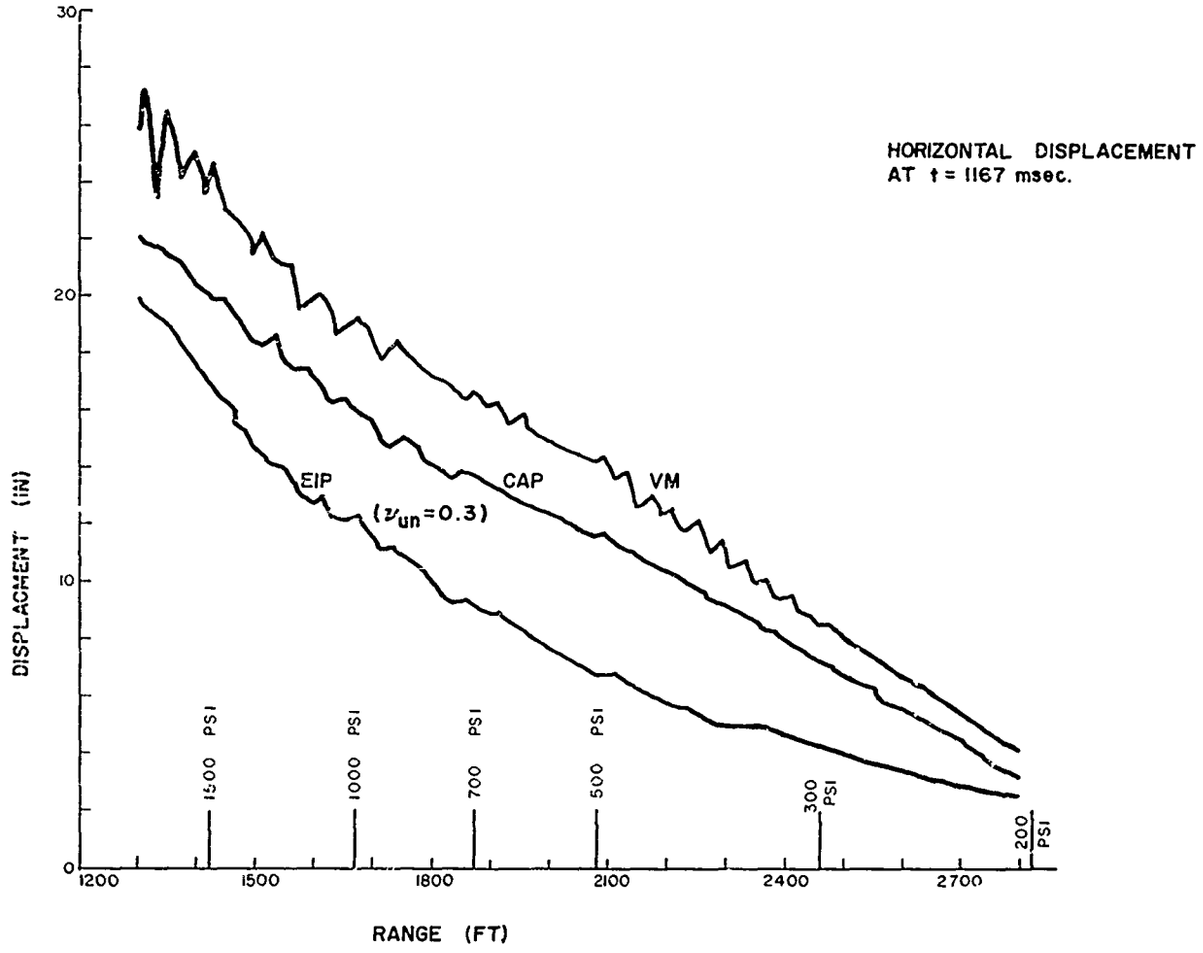

FIG. 5 HORIZONTAL DISPLACEMENT VS. RANGE - DEPTH 30 FT
1 MT AT HOB = 1500 FT

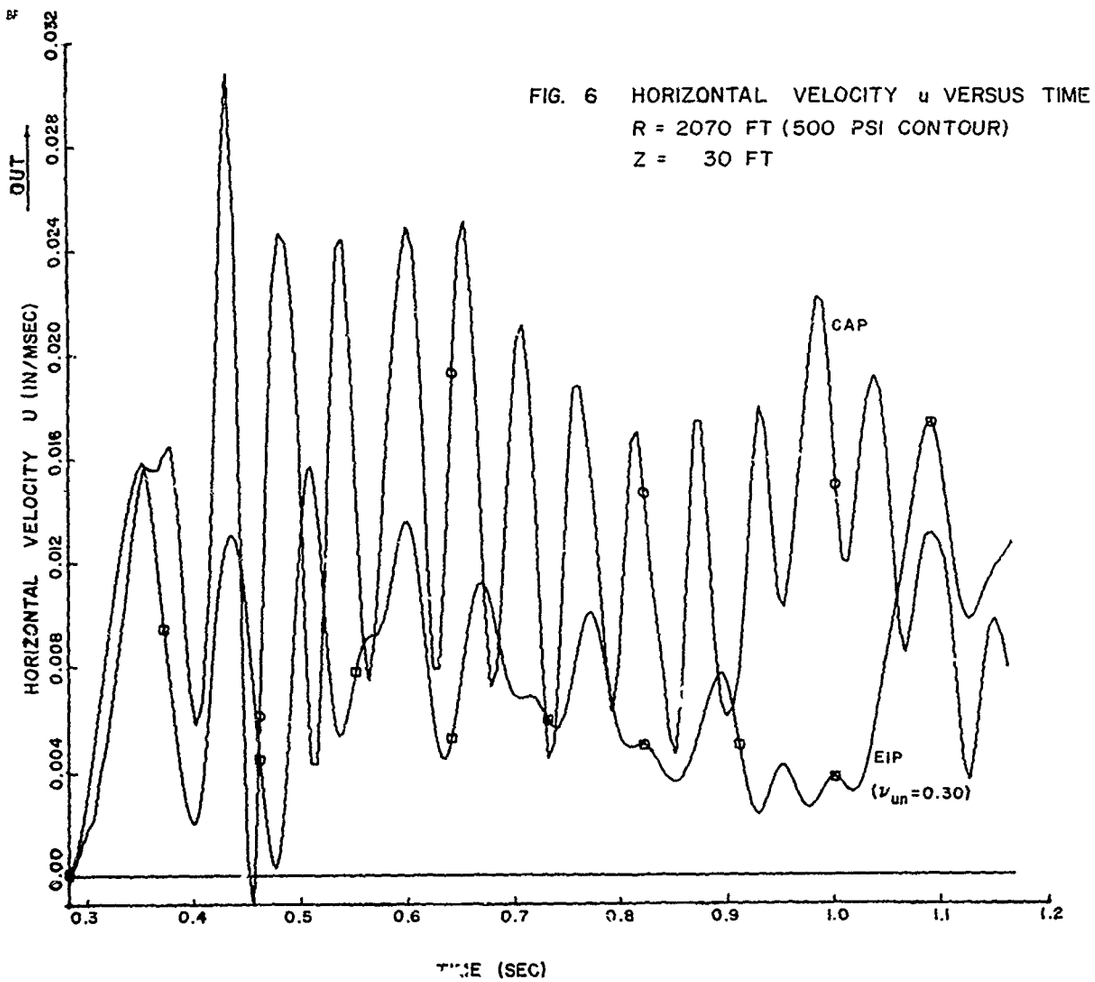

FIG. 6 HORIZONTAL VELOCITY u VERSUS TIME
R = 2070 FT (500 PSI CONTOUR)
Z = 30 FT

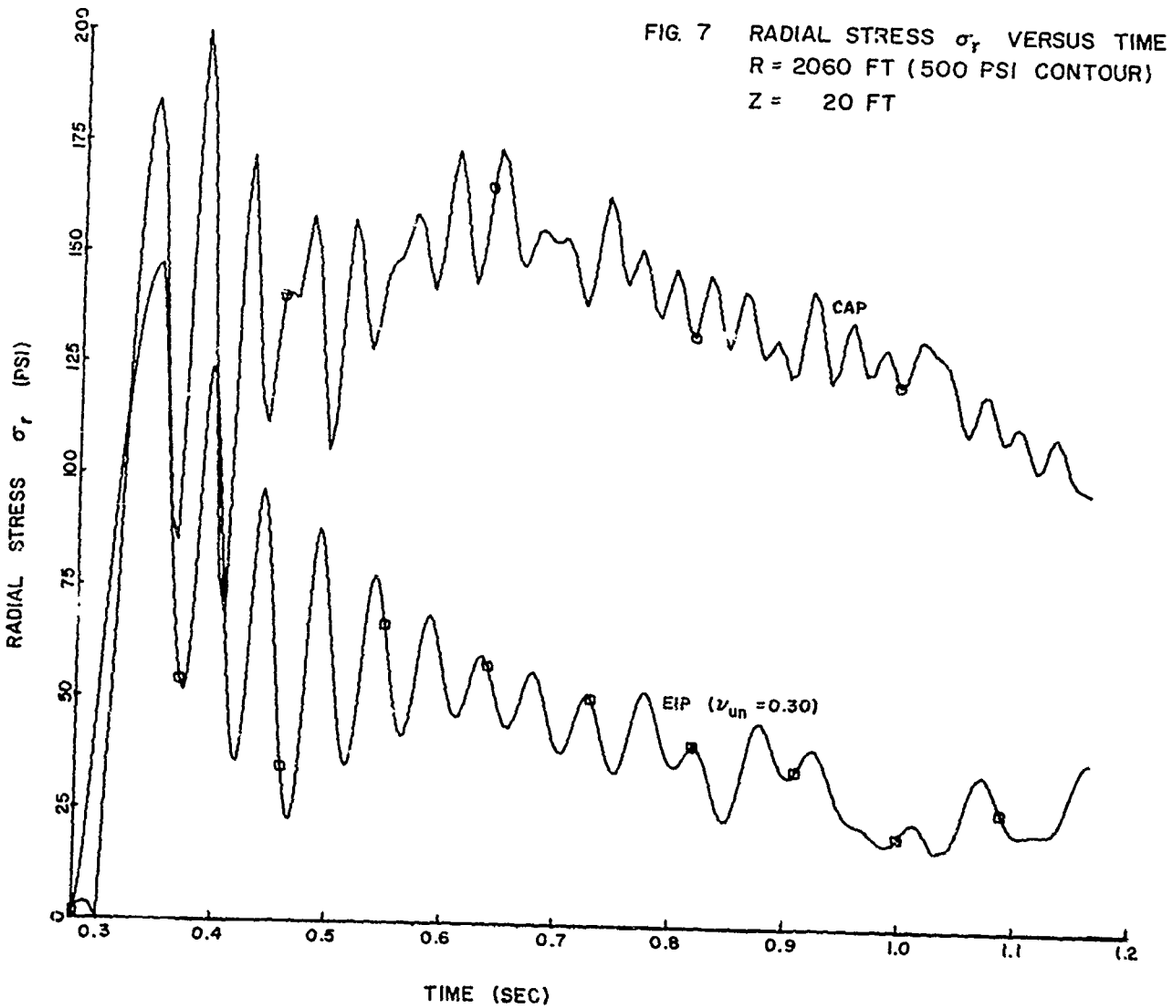

FIG. 7 RADIAL STRESS σ_r VERSUS TIME
R = 2060 FT (500 PSI CONTOUR)
Z = 20 FT

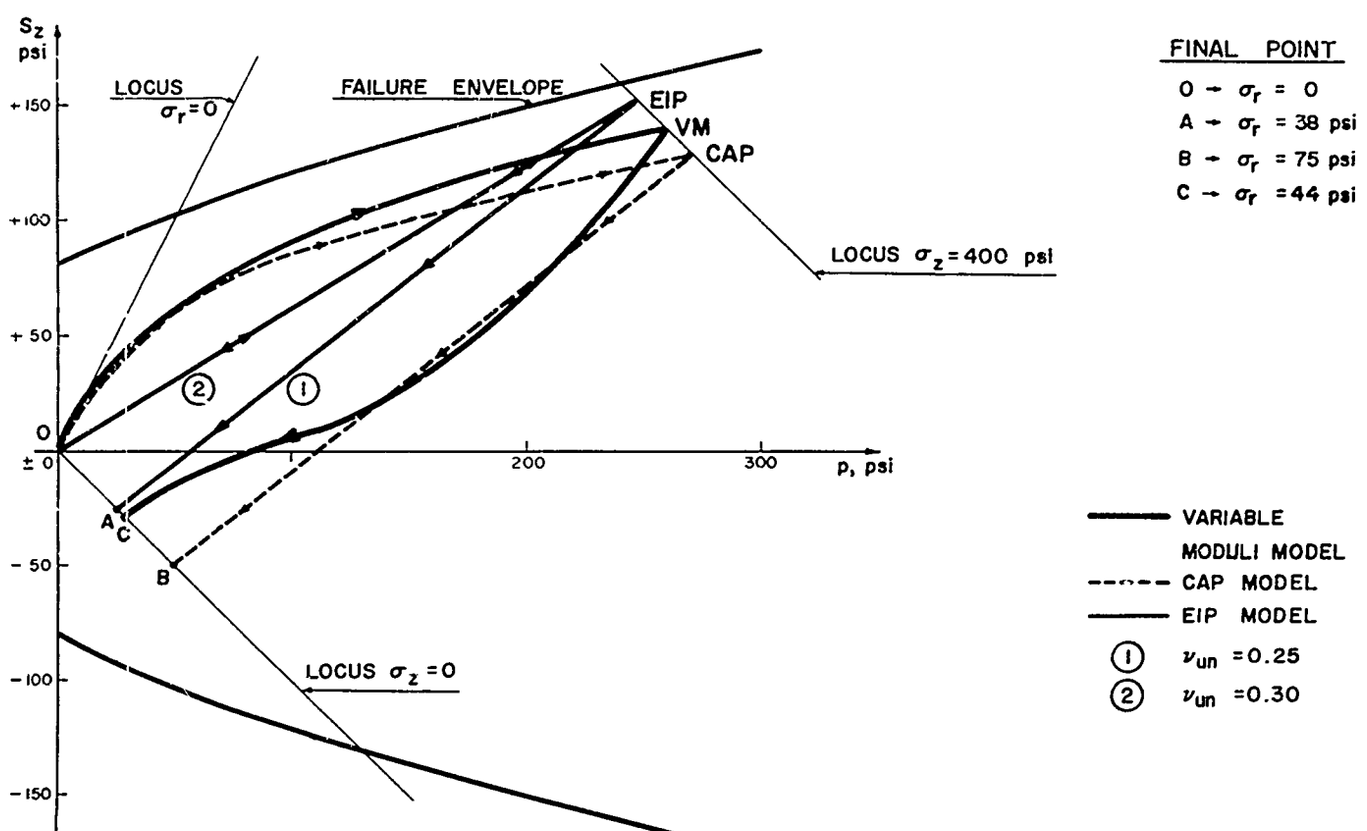

FIG. 8 COMPARISON OF CAP AND ELASTIC-IDEALLY PLASTIC MODELS STRESS PATH FOR UNIAXIAL STRAIN TEST LOADING TO 400 PSI AND UNLOADING.

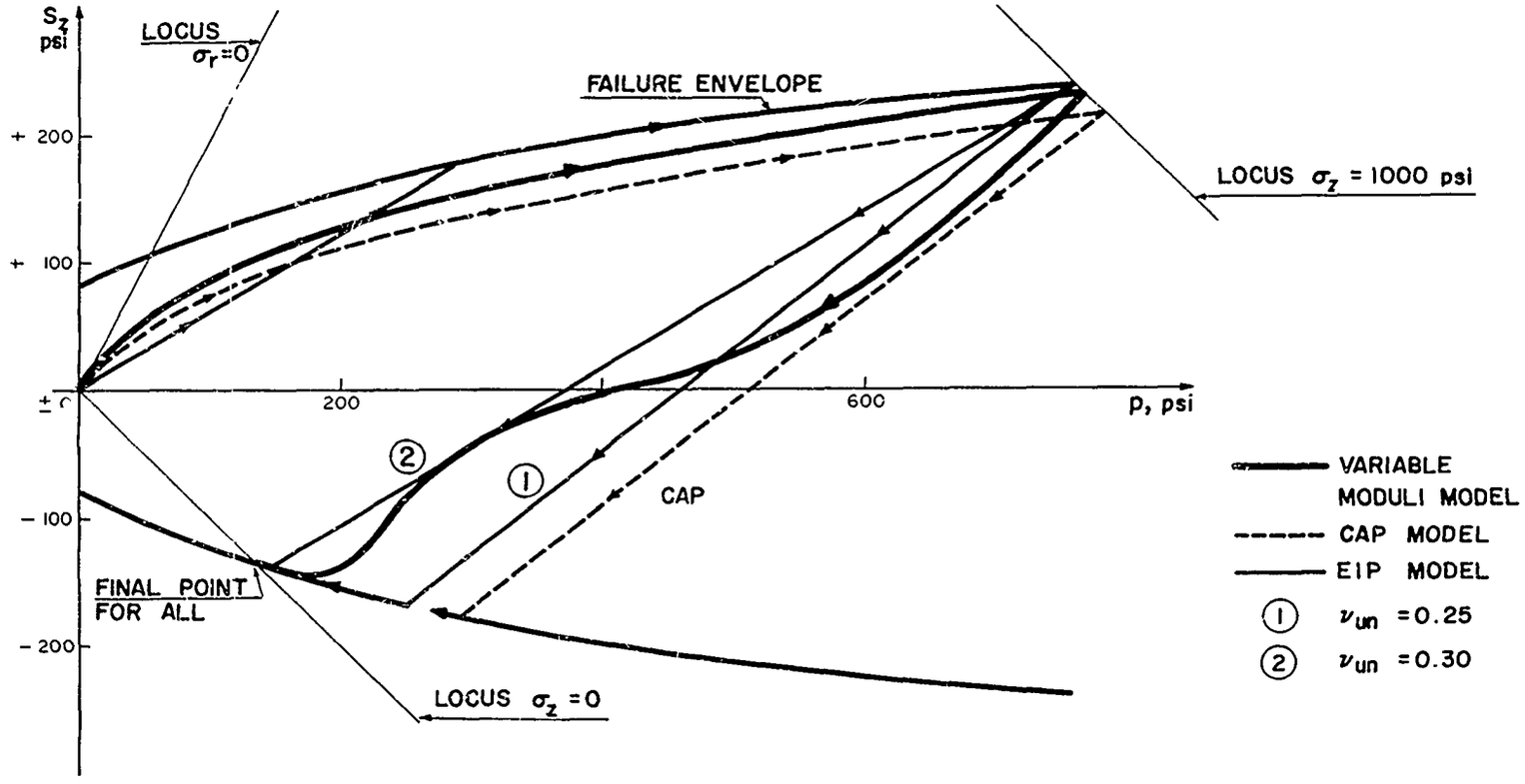

FIG. 9 COMPARISON OF CAP AND ELASTIC – IDEALLY PLASTIC MODELS STRESS PATH FOR UNIAXIAL STRAIN TEST LOADING TO 1000 PSI AND UNLOADING.

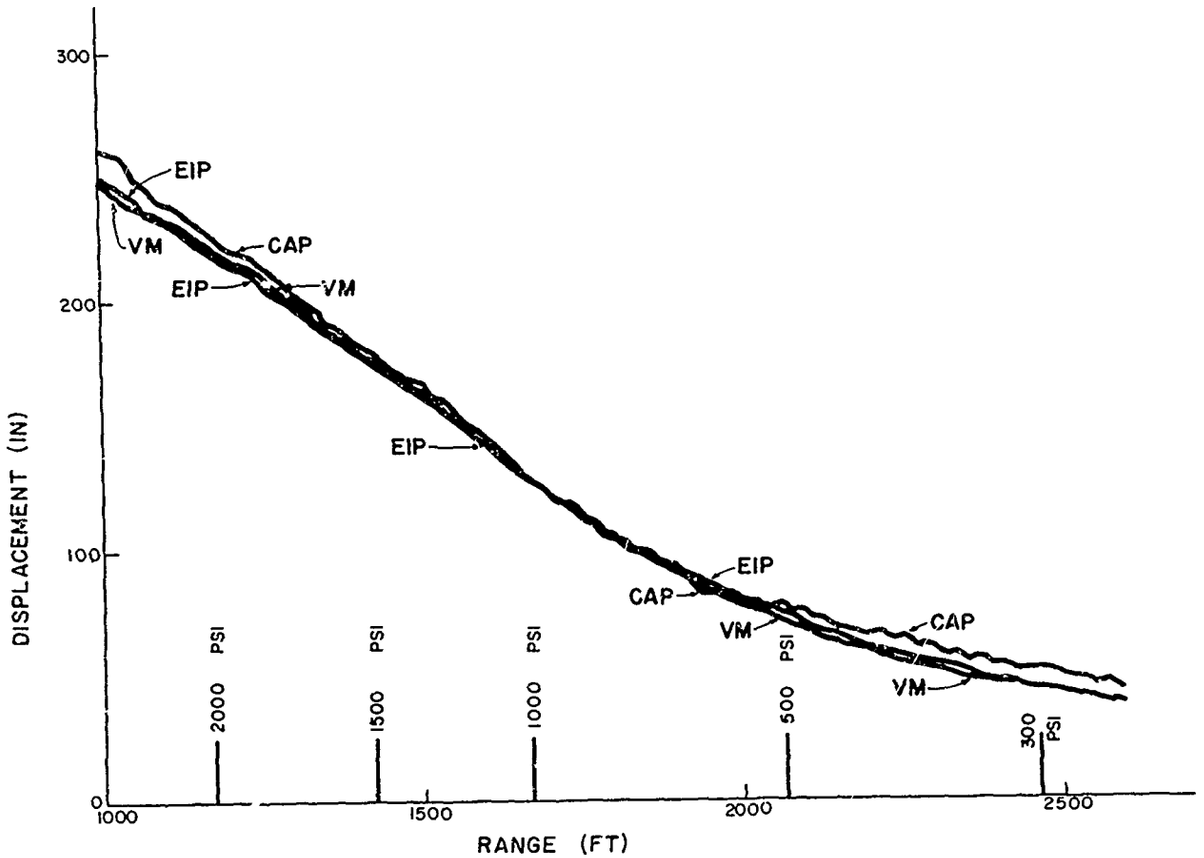

FIG. 10 MAXIMUM VERTICAL DISPLACEMENT VS. RANGE - DEPTH 30 FT
IMT - 1500 FT HOB

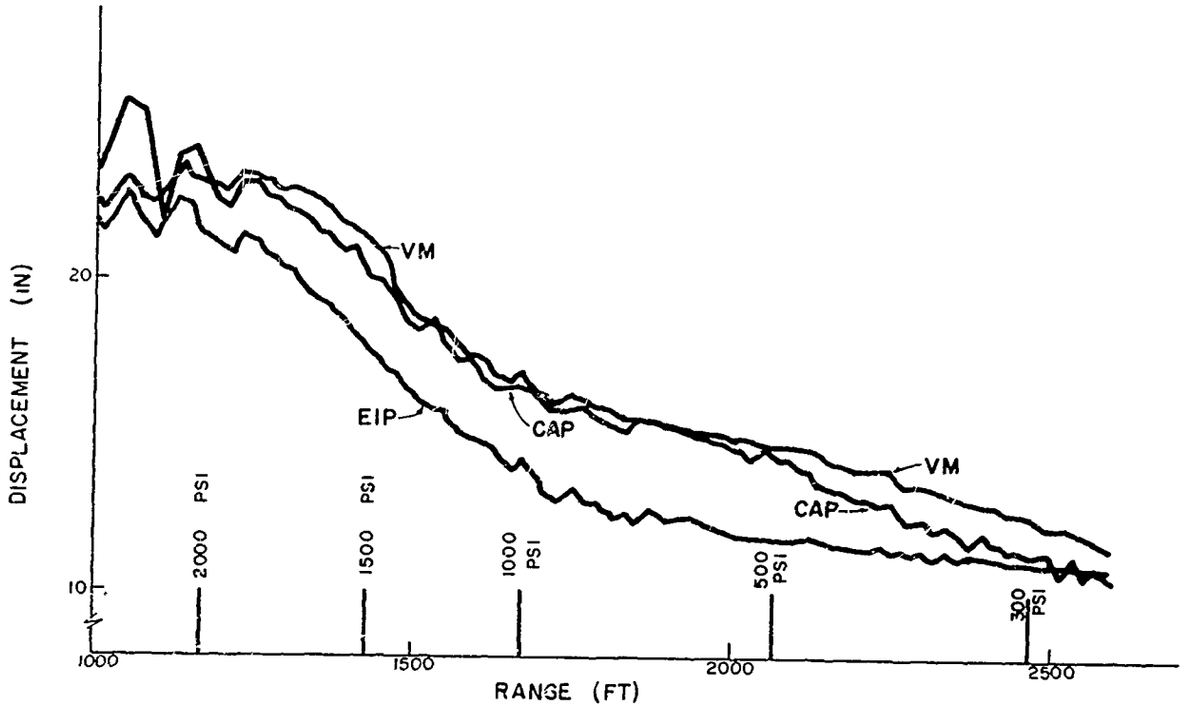

FIG. 11 MAXIMUM HORIZONTAL DISPLACEMENT VS. RANGE - DEPTH 30 FT.
IMT- 1500 FT HOB

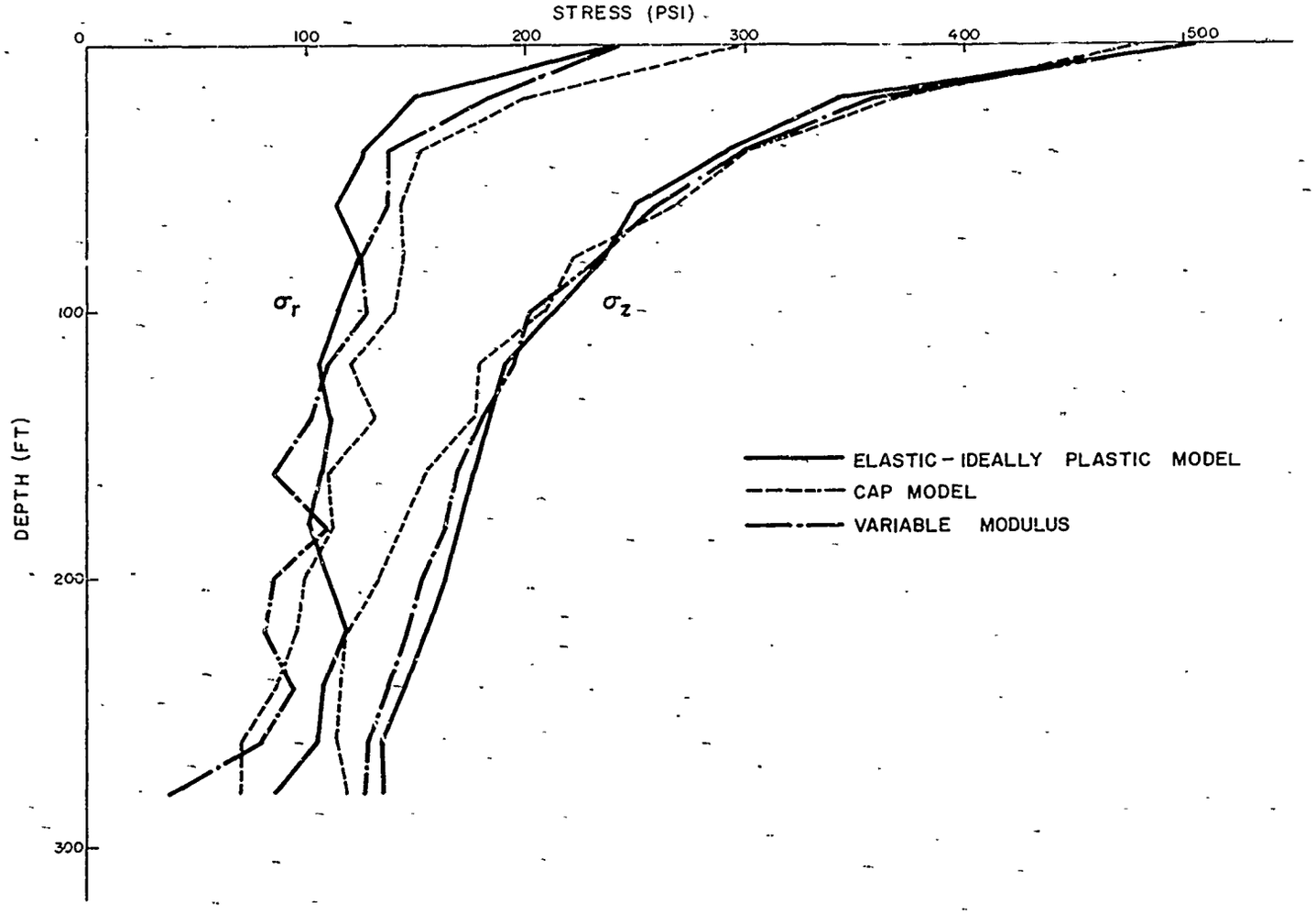

FIG. 12 ATTENUATION OF STRESS WITH DEPTH - 500 PSI CONTOUR

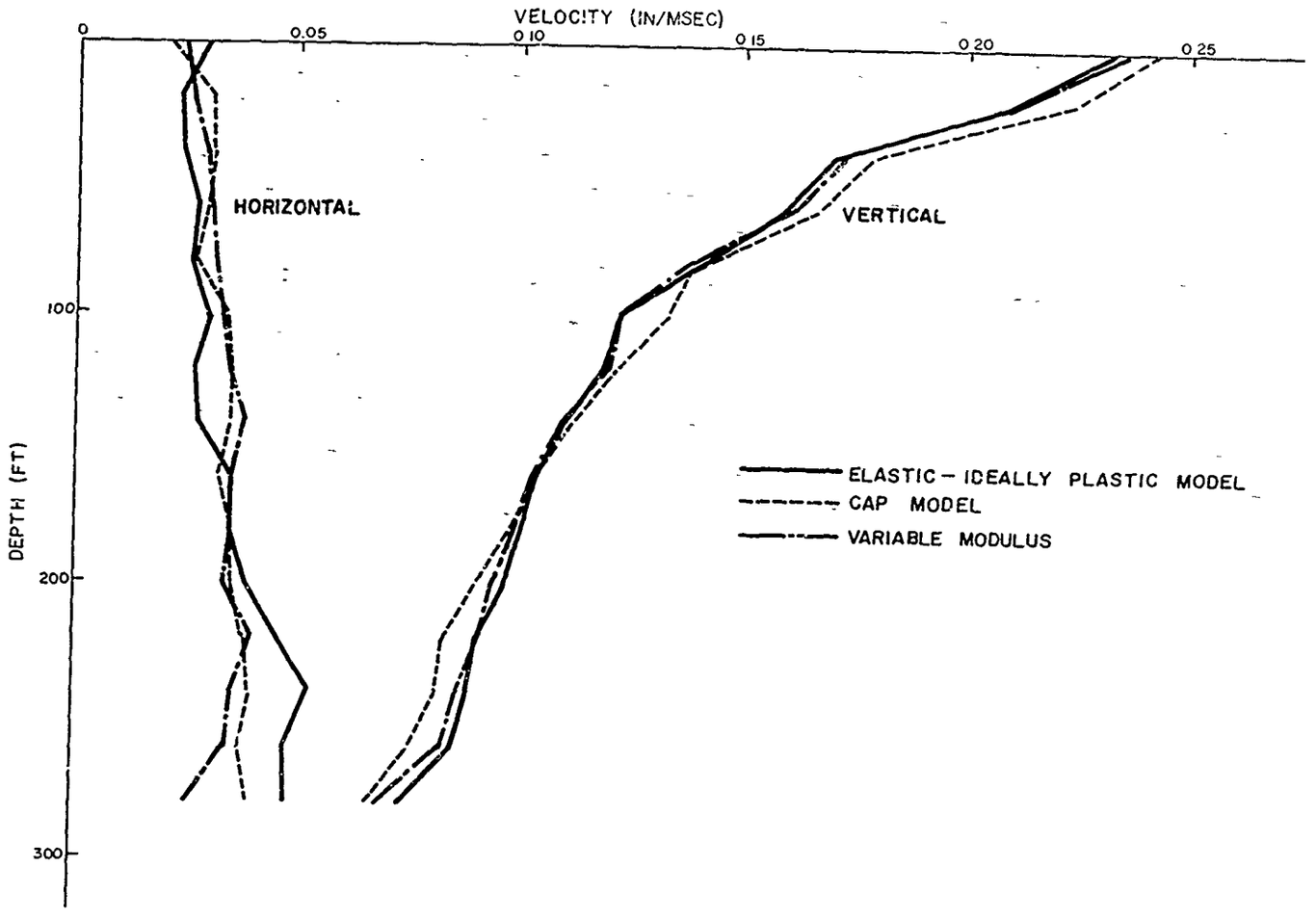

FIG. 13 ATTENUATION OF VELOCITY WITH DEPTH - 500 PSI CONTOUR

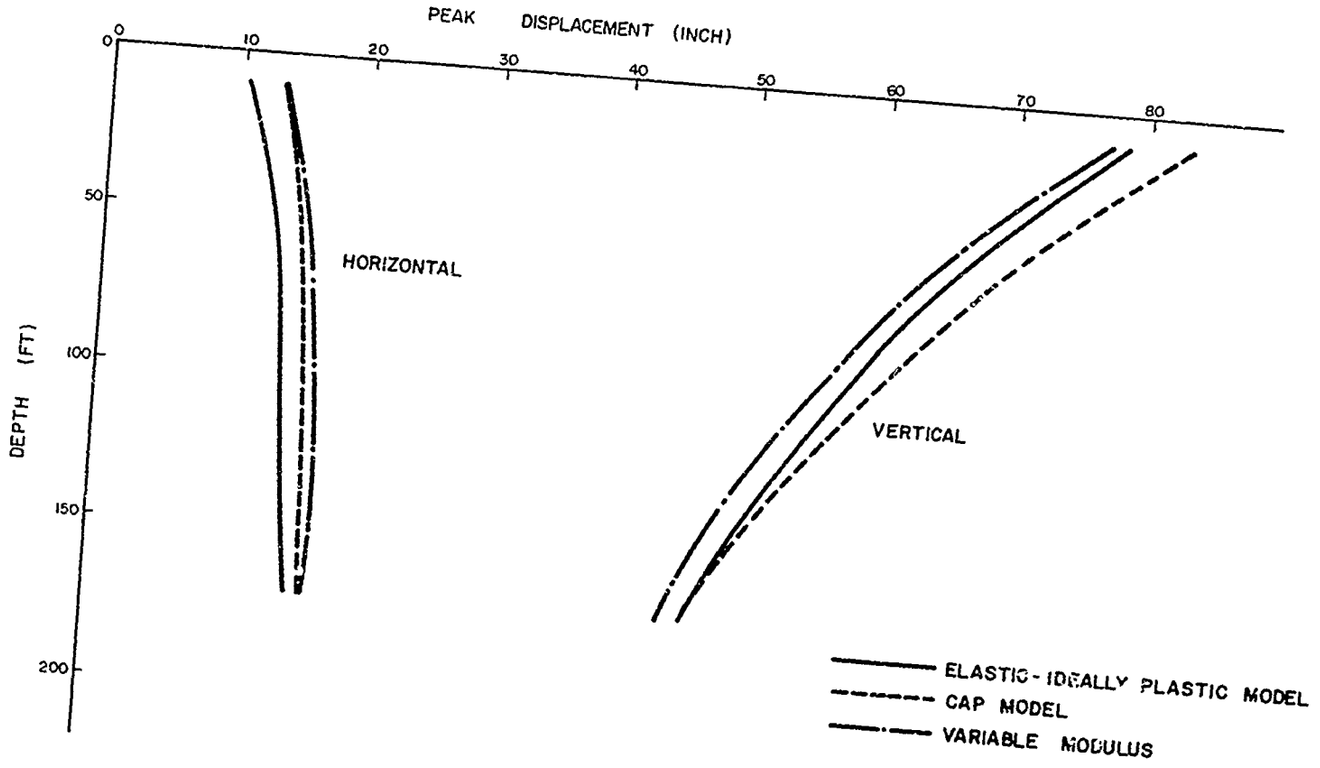

FIG. 14 HORIZONTAL AND VERTICAL DISPLACEMENT VERSUS DEPTH AT 500 PSI CONTOUR

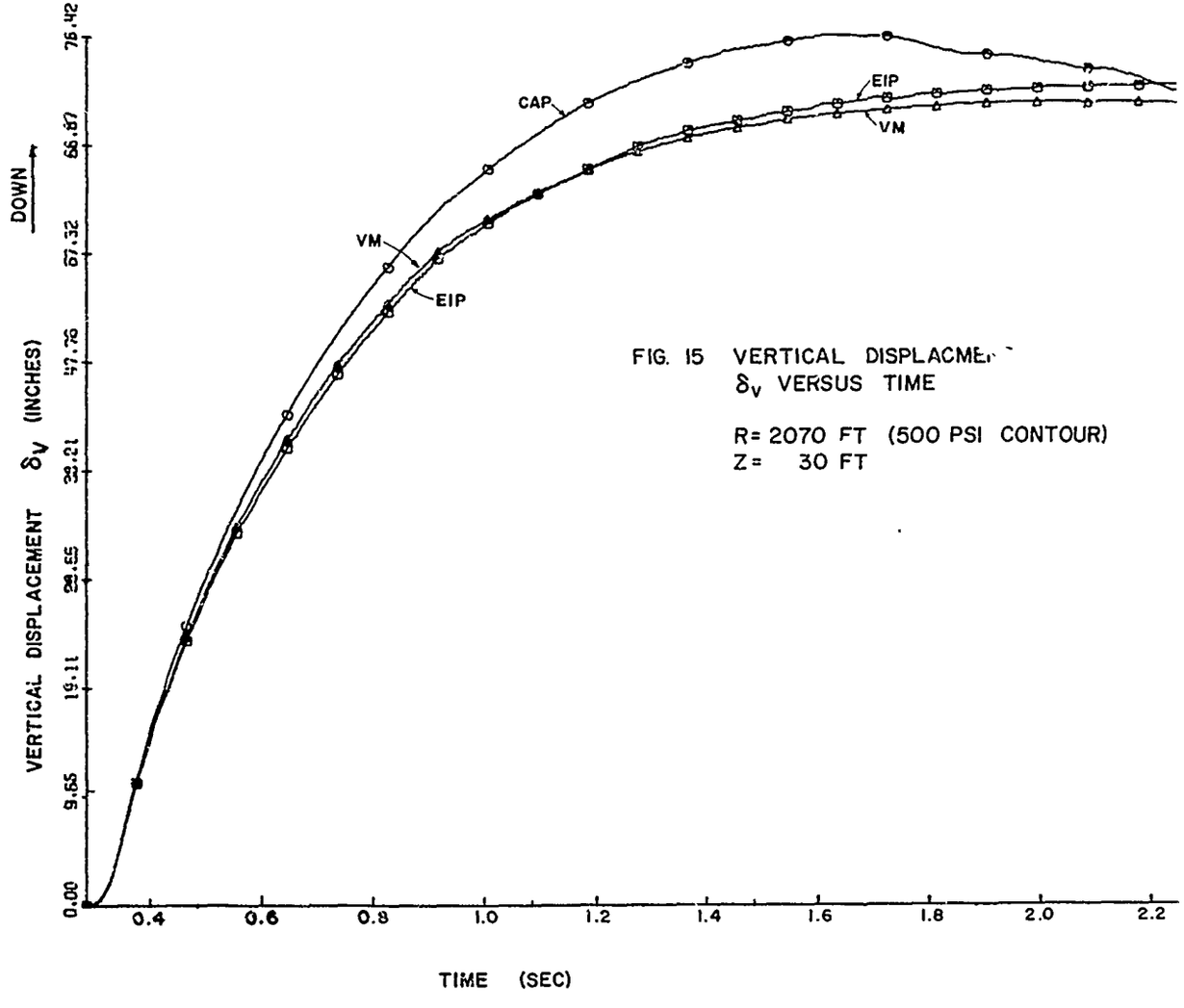

FIG. 15 VERTICAL DISPLACEMENT δ_V VERSUS TIME

R= 2070 FT (500 PSI CONTOUR)
Z= 30 FT

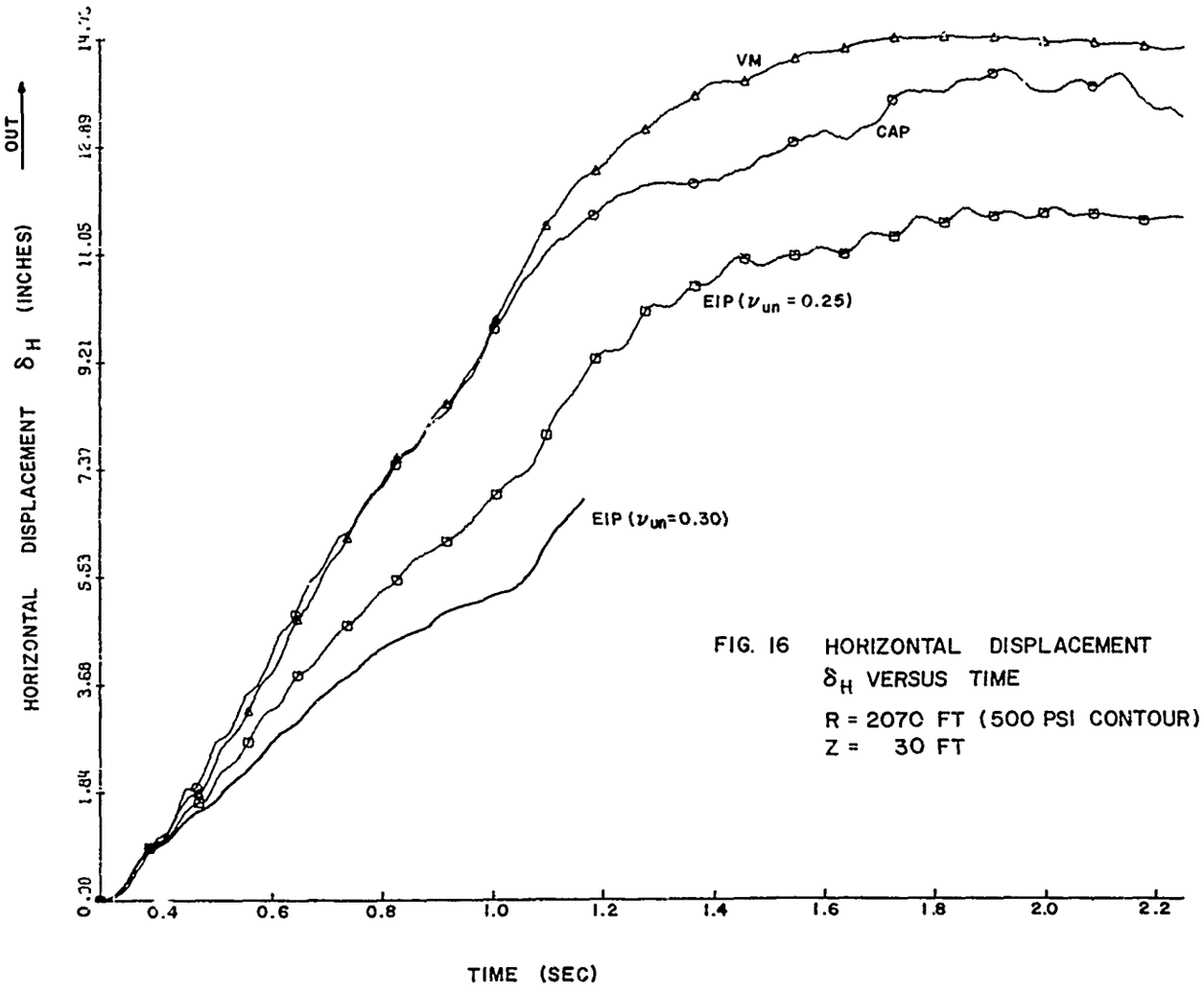

FIG. 16 HORIZONTAL DISPLACEMENT δ_H VERSUS TIME

R = 2070 FT (500 PSI CONTOUR)
Z = 30 FT

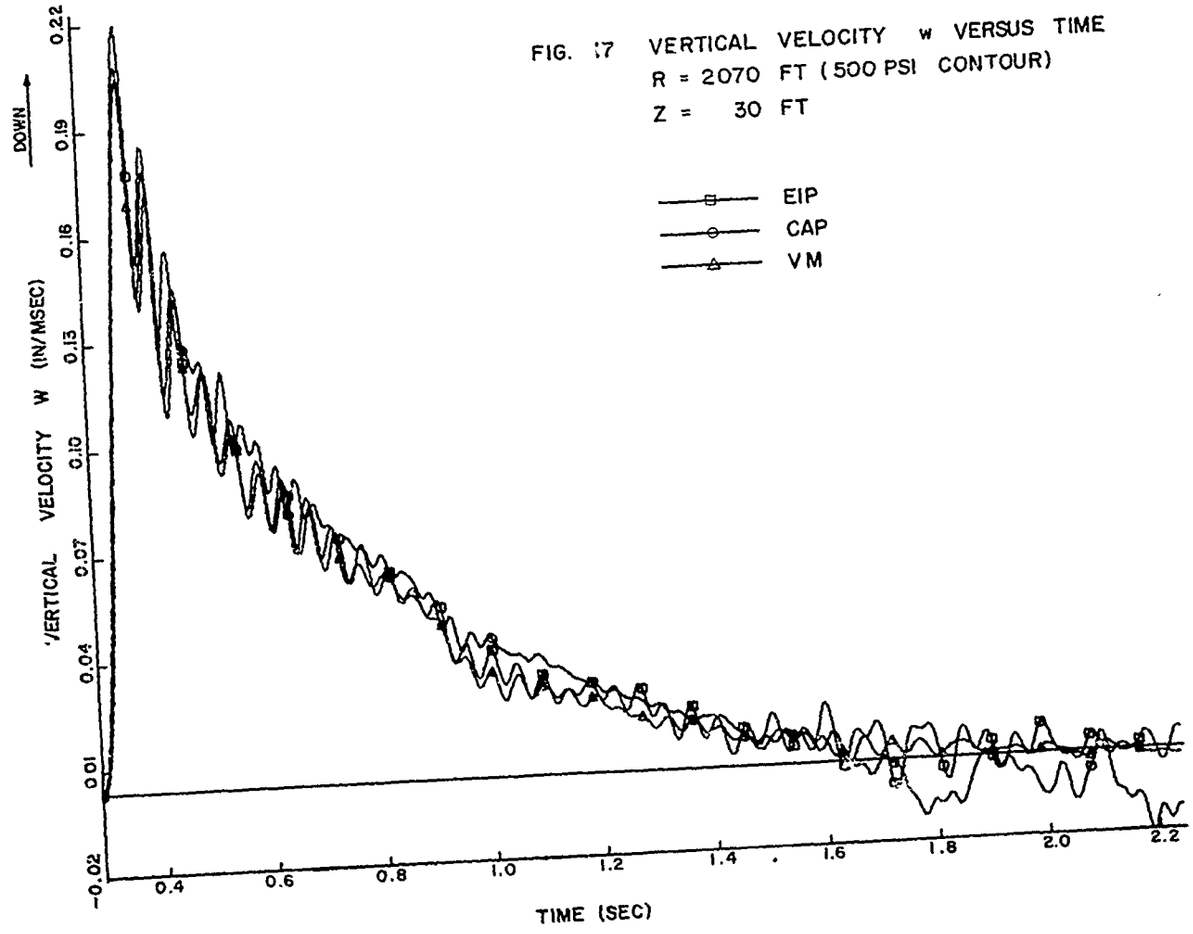
FIG. 17 VERTICAL VELOCITY w VERSUS TIME
R = 2070 FT (500 PSI CONTOUR)
Z = 30 FT
EIP
CAP
VM
DOWN
VERTICAL VELOCITY W (IN/MSEC)
0.22
0.19
0.16
0.13
0.10
0.07
0.04
0.01
-0.02
0.4
0.6
0.8
1.0
1.2
1.4
1.6
1.8
2.0
2.2
TIME (SEC)

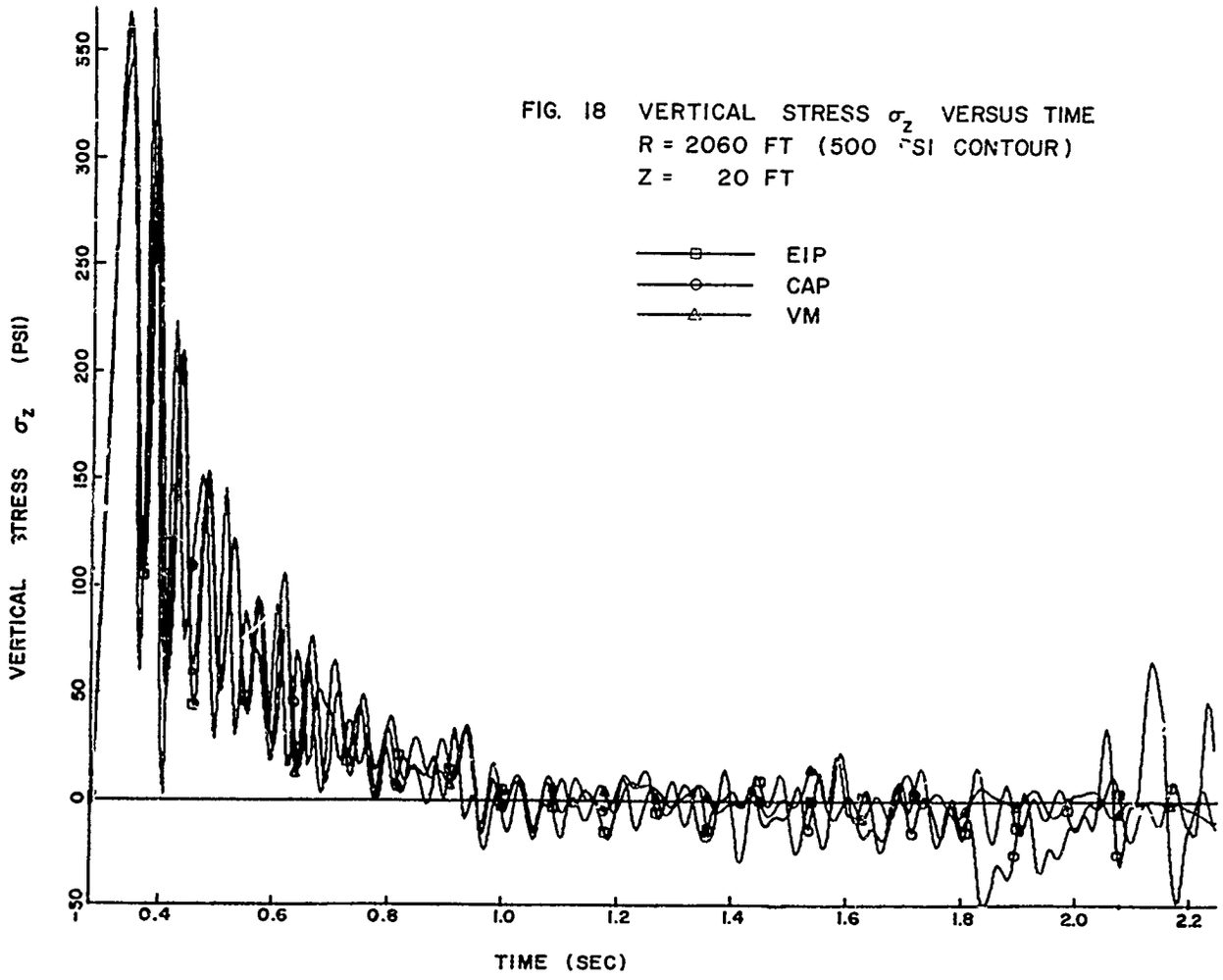

FIG. 18 VERTICAL STRESS σ_z VERSUS TIME
R = 2060 FT (500 PSI CONTOUR)
Z = 20 FT

FIG. 19 RADIAL STRESS σ_r VERSUS TIME
R = 2060 FT (500 PSI CONTOUR)
Z = 20 FT

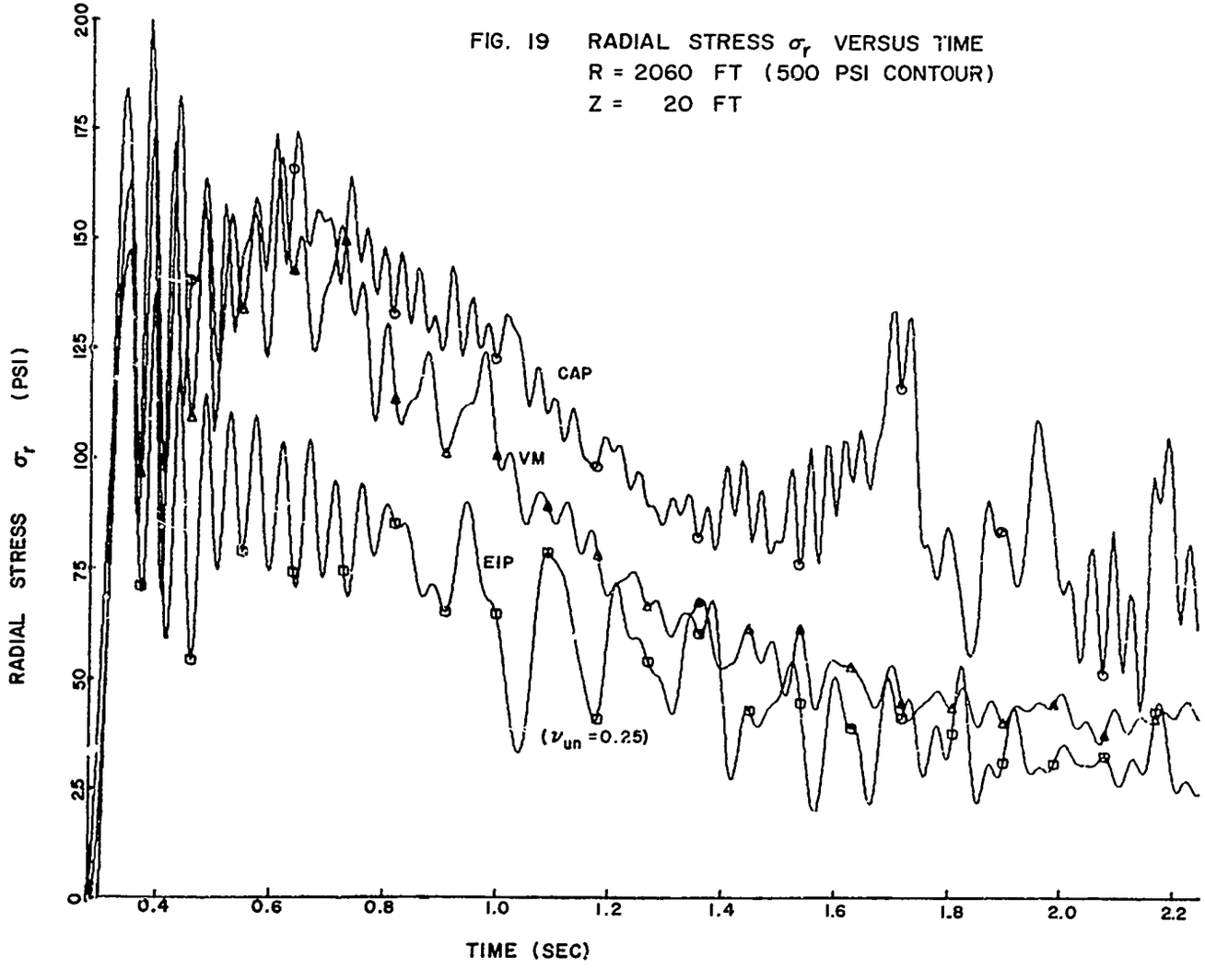

FIG. 20 HORIZONTAL VELOCITY u VERSUS TIME
R = 2070 FT. (500 PSI CONTOUR)
Z = 30 FT.

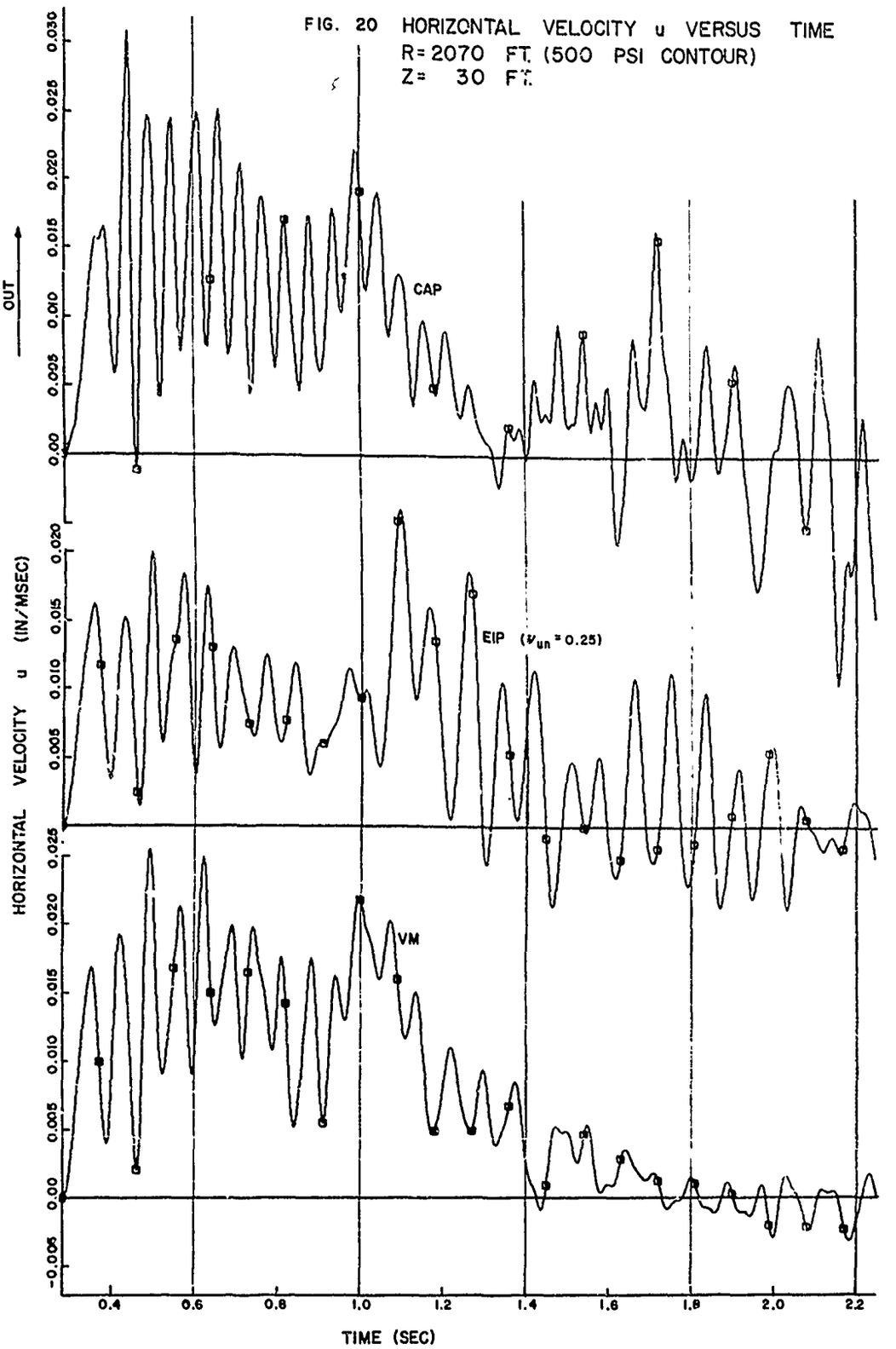

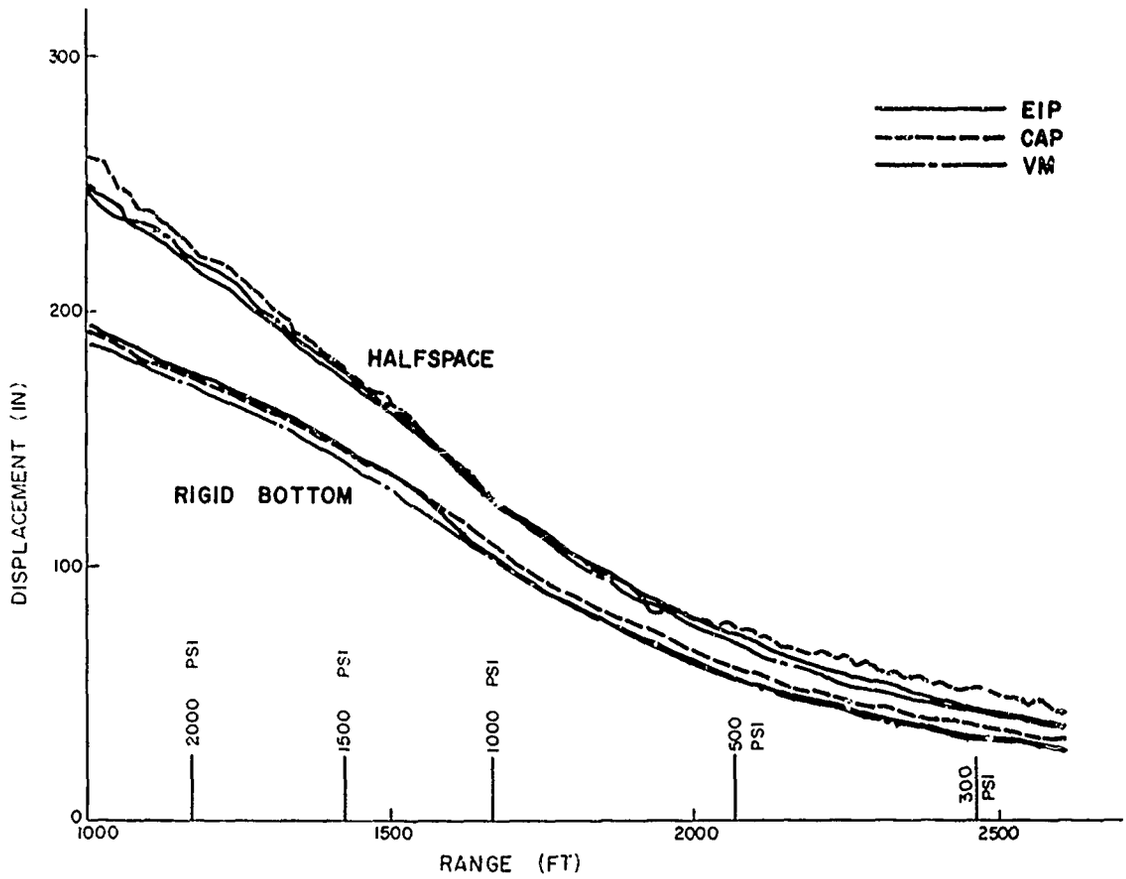

FIG. 21 MAXIMUM VERTICAL DISPLACEMENT VS. RANGE - DEPTH 30 FT
EFFECT OF RIGID BOTTOM

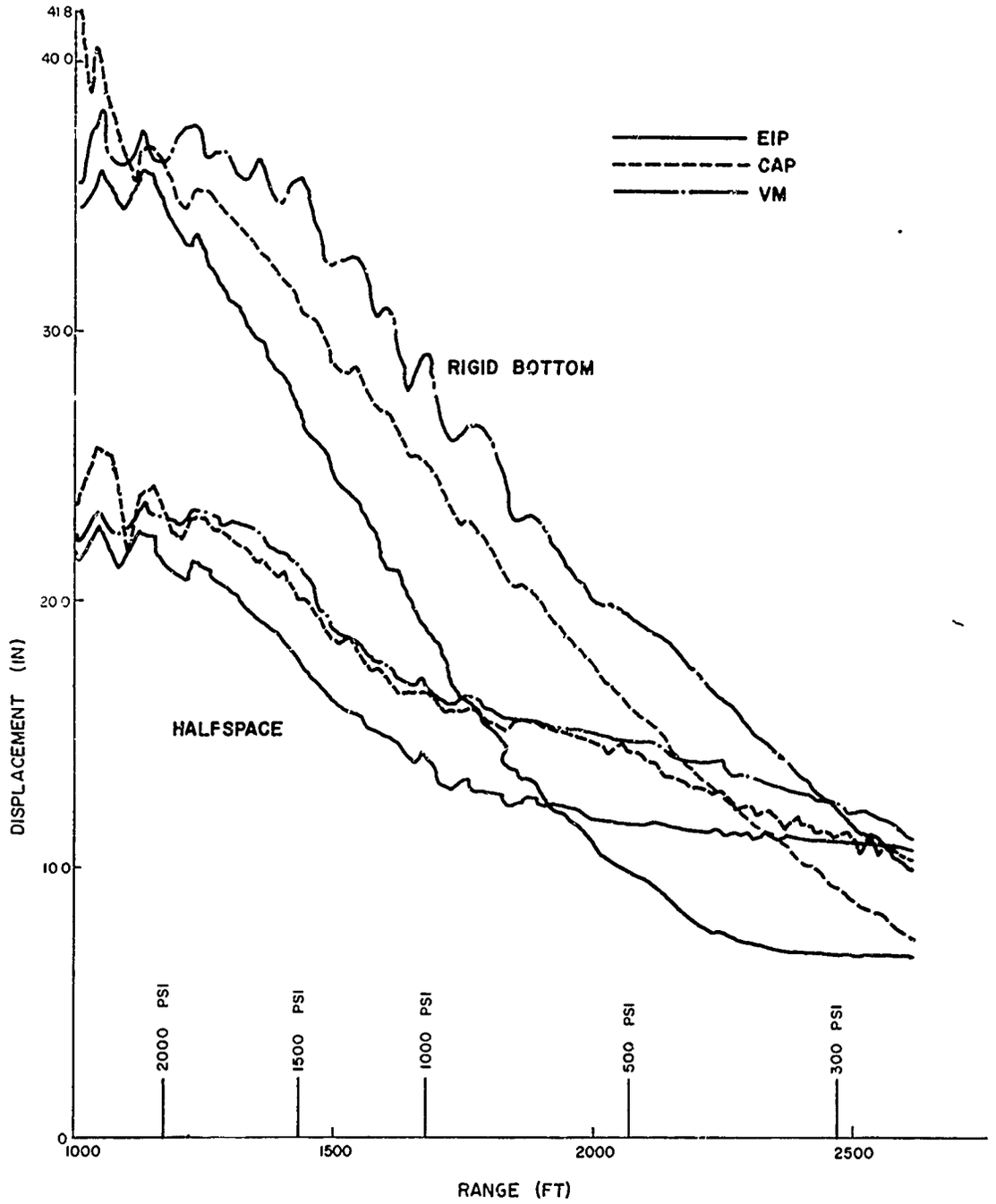

FIG. 22 MAXIMUM HORIZONTAL DISPLACEMENT VS. RANGE - DEPTH 30FT
EFFECT OF RIGID BOTTOM